Effect of breakup on the fusion of ^{6}Li, ^{7}Li, and ^{9}Be with heavy nuclei

M. Dasgupta,[1] P. R. S. Gomes,[2] D. J. Hinde,[1] S. B. Moraes,[2] R. M. Anjos,[2] A. C. Berriman,[1] R. D. Butt,[1] N. Carlin,[3] J. Lubian,[2] C. R. Morton,[1] J. O. Newton,[1] and A. Szanto de Toledo[3]

[1]*Department of Nuclear Physics, Research School of Physical Sciences and Engineering, Australian National University, Canberra, ACT 0200, Australia*

[2]*Instituto de Física, Universidade Federal Fluminense, Av. Litorânea, s/n, Niterói, R.J. 24210-340, Brazil*

[3]*Departamento de Física Nuclear, Instituto de Física, Universidade de São Paulo, Caixa Postal 66318, São Paulo, S.P. 05315-340, Brazil*

(Received 7 May 2004; published 31 August 2004)

Comprehensive high precision complete and incomplete fusion cross sections have been measured for the ^{6}Li+^{209}Bi, ^{7}Li+^{209}Bi, and ^{9}Be+^{208}Pb reactions, at energies near and below the Coulomb barrier. The experimental details and the analyses procedures for the characteristic α-decay and fission measurements are described. Three different methods are used to conclusively show the large suppression of complete fusion at energies around and above the average barrier, which is associated with the projectile nuclei having a low energy threshold against breakup. First, theoretical predictions of fusion cross sections above the average barrier are compared with the data, and second the area under the measured barrier distribution is compared with expectations. The sensitivity of the suppression factors to variables which can affect the calculated cross sections is thoroughly investigated. The third method, essentially model independent, compares the complete fusion cross sections for the ^{7}Li+^{209}Bi and ^{9}Be+^{208}Pb reactions with those for the fusion of nuclei with a high threshold against breakup, which produce the same compound nucleus. All methods give consistent results, showing that the complete fusion cross sections at energies around and above the barrier are suppressed by $\sim$30% compared with reactions of nuclei having a high energy threshold against breakup. The cross sections for incomplete fusion are found to be similar to the missing complete fusion cross sections. The experimental controversies regarding the effect of breakup on fusion is discussed, and the importance of unambiguously separating complete fusion from incomplete fusion is emphasized. This distinction is also important to achieve theoretically for realistic modelling of fusion of nuclei which break up readily.

DOI: 10.1103/PhysRevC.70.024606 PACS number(s): 25.70.Jj, 25.70.Mn, 25.60.Gc, 25.60.Dz

I. INTRODUCTION

The effect on the fusion process of the breakup of weakly bound light nuclei is a subject of current experimental [1–9] and theoretical investigations [10–15]. This is due to the recent availability of beams of unstable nuclei with weakly bound nucleons. An understanding of breakup and fusion is directly relevant to producing nuclei near the drip lines, and possibly super-heavy nuclei. Although it is now possible to investigate reaction mechanisms with these exotic nuclei, experimentally such studies are limited due to the low intensities of unstable beams currently available. Fusion reactions with high intensity stable beams which have a significant breakup probability are good references for testing the models of breakup and fusion currently being developed. Light nuclei such as ^{9}Be, ^{6}Li, and ^{7}Li with low breakup thresholds are ideal as they have a large breakup probability (compared with heavy nuclei with low breakup thresholds) due to the low Coulomb barriers associated with breakup. The nucleus ^{6}Li breaks up into ^{4}He+^{2}H, with separation energy S_{α} = 1.48 MeV; ^{7}Li into ^{4}He+^{3}H, with S_{α} = 2.45 MeV. The Borromean nucleus ^{9}Be can break up into ^{8}Be+$n \rightarrow ^{4}$He+^{4}He +n, with S_{n} = 1.67 MeV or into ^{5}He+^{4}He, with S_{α} = 2.55 MeV. Fusion with the three above mentioned nuclei, with different structures and separation energies, are ideal for quantitative tests of theoretical models. They are also useful as comparators for fusion measurements with unstable beams of ^{11}Li and ^{11}Be.

In this paper we present precise excitation functions for the fusion of ^{6}Li and ^{7}Li with ^{209}Bi, and of ^{9}Be with ^{208}Pb, at energies ranging from 0.9 to 1.7 times the Coulomb barriers. Excitation functions are presented for (*i*) complete fusion (CF)—defined experimentally as the capture of all the charge of the projectile by the target, and (*ii*) incomplete fusion (ICF)—where, following the breakup of the projectile into charged fragments, one of the fragments is captured by the target [6,16,17]. The separation of complete fusion from incomplete fusion is crucial for understanding the effect of breakup on fusion. The target nuclei in the present work were chosen so that the fused system, being heavy and neutron-rich, de-excites overwhelmingly by neutron evaporation, and the residues formed following CF and ICF are alpha active, with lifetimes such that most of the alpha activity could be measured during or shortly after irradiation. The measurement of characteristic decay alpha particles allows the unambiguous identification of CF and ICF products. Selected results from this work have been reported previously [6,9]. In this paper we give the details of the experiment, analysis and present the cross sections for each CF and ICF product nucleus.

II. THE EXPERIMENTAL METHOD

The experiments were performed using the 14UD tandem accelerator at the Australian National University. Beams of

TABLE I. Beam characteristics, monitor angles, and reaction products measured.

Reaction	E_{beam} (E_{step}) (MeV)	Monitor angle	Pulsing on:off	Products measured
^{6}Li+^{209}Bi	26.0−34.0 (1.0)	±17.2°	1 ns:533 ns	$^{211-213}$Rn, fission, $^{211-213}$At, ^{211,212}Po
	36.0−40.0 (2.0), 44.0, 48.0	±17.2°	1 ns:533 ns	as above, ^{210}Rn
	30.0−38.0 (4.0)	±15.0°	d.c.	^{210,208}Po
	44.0, 48.0	±15.0°	10.7 ms:21.3 ms	$^{210-212}$Rn, ^{211,212}At ^{211,210,208}Po
	48.0	±13.35°	1 ns:640 ns	as above and ^{213}Rn
^{7}Li+^{209}Bi	25.0−36.0 (1.0)	±17.2°	1 ns:533 ns	$^{212-214}$Rn, fission ^{211,212}Po, $^{211-213}$At, ^{211}Bi
	38.0, 40.0−52.0 (4.0)	±17.2°	1 ns:533 ns	as above, ^{210,211}Rn and ^{210}Po
	30.0, 34.0	±15.0°	d.c.	^{210}Po
	30.0, 33.0−39.0 (2.0), 48.0	±13.35°	1 ns:640 ns	$^{211-213}$Rn, ^{211}Po, ^{211}At
^{9}Be+^{208}Pb	36.0−51.0 (1.0)	±22.5°	1 ns:1 μs	$^{213-215}$Rn, ^{211,212}Po, fission
	45.0−51.0 (3.0)	±17.2°	1 ns:533 ns	^{212}Rn, ^{210}Po
	38.0, 41.0, 43.0	±17.2°	d.c.	^{210}Po

^{6}Li, ^{7}Li, and ^{9}Be were incident on self-supporting ^{nat}Bi and enriched (>99%) ^{208}PbS targets evaporated onto 15 μg/cm^2 C foils. Recoiling evaporation residues were stopped in aluminum catcher foils placed immediately behind the targets. Two Si surface barrier detectors (monitors), placed above and below the beam axis, were used to measure the elastically scattered beam particles, for normalization purposes. The angles of these detectors (see Table I) were chosen so that (*i*) elastic scattering from Bi/Pb could be separated from elastic scattering from low *Z* elements in the target, and from the catcher foils, and (*ii*) elastic scattering would be purely Rutherford. Most of the measurements were done with pulsed beams, with laboratory energies ranging from 26.0 to 52.0 MeV. Table I shows the beam energies, pulsing regimes, and the reaction products measured in these experiments. The fusion reactions ^{6}Li+^{209}Bi, ^{7}Li+^{209}Bi, and ^{9}Be +^{208}Pb lead to the compound nuclei ^{215}Rn, ^{216}Rn, and ^{217}Rn, respectively. These nuclei de-excite mainly by neutron evaporation, with some fission. The residual Rn nuclei are near the $N=126$ and $Z=82$ closed shells, and are alpha active. The products of incomplete fusion, Po and At isotopes for ^{6,7}Li induced reactions, and At isotopes for the ^{9}Be reaction, are also alpha active. The cross sections for residues resulting from complete and incomplete fusion were determined by measuring their alpha activity as discussed in the next sub-section. The fission cross sections were determined by direct detection of the fission fragments, as described in Sec. II B.

A. Decay alpha measurements

The experimental setup for the decay alpha measurements is shown in Fig. 1(a). The catcher foils, placed immediately behind the target to stop the recoiling heavy reaction products, had thicknesses of 180 μg/cm^2 and 360 μg/cm^2 for the Li and Be induced reactions, respectively. These thicknesses are more than 1.5 times the mean range of the recoiling nuclei. The nuclei were identified by their characteristic α particle energies and decay half lives, which ranged from 110 ns to 138 days. Alpha particles from the short-lived activities, ranging from 110 ns to 23.1 min, were detected between the beam pulses using an annular silicon surface barrier detector, placed 8 cm from the target, at a mean angle of 174° to the beam. Alpha decays from long-lived activities, ranging from 23.1 min to 138 days, were measured using a

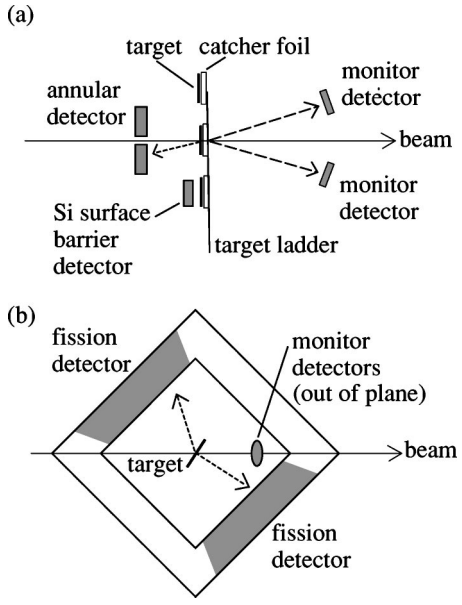

FIG. 1. Detector configurations for (a) the decay α measurements, and (b) the measurement of the fission fragments.

silicon surface barrier detector below the annular counter, placed so that when the target and catcher foil were moved down one target position after the irradiation, they were only 0.8 cm from the detector face [see Fig. 1(a)]. Absolute cross sections were determined by measuring sub-barrier elastic scattering in the annular detector and monitors. The relative solid angle between the annular and the close geometry α-detector was determined by measuring the ^{212}Rn decay ($T_{1/2}$=23.1 min) in both the detectors. Fresh targets were used at each energy, except for a few energies where previously irradiated targets were used. For the latter cases, small corrections were made to the α yields to account for previous irradiation. Typically, at the end of irradiations, the following decay spectra were collected: (a) ~2 min after the irradiation for a duration of ~10 min, (b) ~15 min after the irradiation for a period of ~40 min, (c) ~1 day after the irradiation for a period of about 1 h, and finally (d) a few days after the irradiation for a period of several hours to detect very long lived activity. These decay spectra enabled determination of cross sections for direct population by ICF of nuclei which are members of decay chains and are also populated through decay of the parent nuclei. The measurements of type (d) were not done at all energies, and were only used to determine the cross sections of ^{210}Po ($T_{1/2}$=138 days).

B. Fission measurements

Fission following fusion was measured during the irradiations using two large area (28.4×35.7 cm^2) two dimensional position sensitive multi-wire proportional counters [18], as shown in Fig. 1(b). The detectors [19,20] were placed at a distance of 18.0 cm from the target. Each detector, with a position resolution of 1 mm, covered an angular range of 75° ($-95° \geqslant \theta_{lab} \geqslant -170°$ in the backward hemisphere and $10° \leqslant \theta_{lab} \leqslant 85°$ in the forward hemisphere), allowing the determination of the cross section in one measurement. Signals in the forward detector were only accepted when in coincidence with the backward detector. Detailed descriptions of the fission product selection and the fission cross section determination can be found in Refs. [19–21]. Absolute fission cross sections were determined by performing calibrations at sub-barrier energies [21], by the detection of elastically scattered heavy projectiles (e.g. ^{58}Ni,^{63}Cu) in the multi-wire proportional counters and monitor detectors. The large solid angle of the fission detectors, compared with the solid angle of the annular counter, allowed the measurement of angular distributions with high statistics and consequently small uncertainties, despite the small fission cross sections.

III. ANALYSIS OF ALPHA SPECTRA

Figure 2 shows α-particle spectra for ^{9}Be+^{208}Pb, collected during irradiation at two energies, one ≃2 MeV below the Coulomb barrier, and the other 10 MeV above the barrier. The α-particles from CF (Rn nuclei) and ICF (Po nuclei) are identified. The change in the dominant evaporation channel from 3n (^{214}Rn) to 4n (^{213}Rn) with an increase in energy is clearly seen. The individual peak shapes of the α-spectrum and their detected energies are determined by the energy

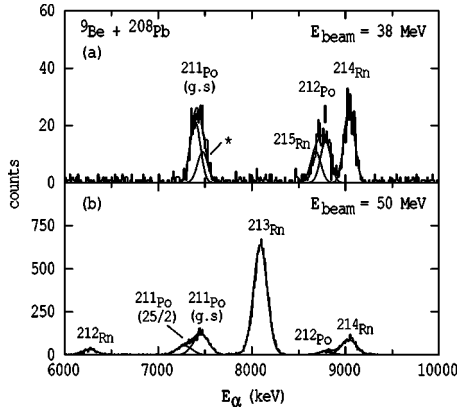

FIG. 2. Measured α-spectra for the ^{9}Be+^{208}Pb reaction collected during irradiation at beam energies of (a) 38 MeV, which is ≃2 MeV below the fusion barrier, and (b) 51 MeV, which is ≃10 MeV above the fusion barrier. The full lines are fits to the α-spectrum. All the peaks can be clearly identified, and the peak marked with an asterisk is from the decay of ^{211}Po which is formed by the decay of ^{211}Rn (see the text).

losses experienced by the α-particles. This arises because the decay products are implanted to a range of depths in the catcher foil due to (i) the finite thickness of the target foils, and (ii) the mechanism of CF and ICF leading to different energies of the recoiling nuclei. Figure 3 shows the α-spectra for the ^{7}Li+^{209}Bi reaction at an energy E_{beam}=52 MeV collected (a) during irradiation, (b) commencing 3.2 min after the irradiation, and (c) 42.5 h after the irradiation. The α-decay of the CF and ICF products are identified in Fig. 3(a), along with those from the high spin isomeric states of ^{211}Po and ^{212}At. The offline spectrum in Fig. 3(b) is dominated by the decay α from ^{212}Rn ($T_{1/2}$=24 min) although the

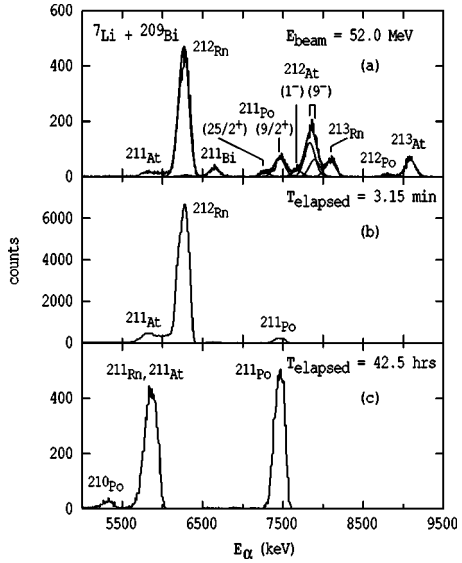

FIG. 3. Typical measured α-spectra for the ^{7}Li+^{209}Bi reaction for a beam energy of 52 MeV. (a) Collected during the irradiation, (b) off-line measurement commencing 3.2 min after the end of irradiation, and (c) off-line measurement commencing 42.5 h after the irradiation. The full lines in panel (a) are the results of a fit (see the text).

lines from the ^{211}At ($T_{1/2}$=7.2 h) decay chain are also visible. The strongest peaks in Fig. 3(c) result from the decay of ^{211}Rn ($T_{1/2}$=14.6 h)$\rightarrow$^{211}At$\rightarrow$^{211}Po. This spectrum also shows the α-line from the decay of ^{210}Po ($T_{1/2}$=138 days).

The α-spectra were fitted using the peak-fitting program FITEK [22]. The energy calibration for the α-spectrum was determined for each bombarding energy using isolated and intense lines, such as those resulting from 3*n* evaporation and 4*n* evaporation. The energy differences between the α-lines resulting from CF were fixed with respect to the strongest CF peak. The same was done for incomplete fusion products. The CF and ICF peaks were grouped separately to account for the small differences which may exist in the implantation depth of the recoiling nuclei resulting from CF and ICF. This effect can most clearly be seen in Fig. 2(b), where the peak corresponding to the decay of ^{211}Po has two components: one from ^{211}Po populated through ICF (lower detected energy), and the second from ^{211}Po populated via CF (marked with asterisk in the spectrum). In cases where the residual nucleus decays by more than one α-energy, the known branching ratio was used to fix their relative intensities. Having thus fixed the relative energy differences and relative intensities, the fitting routine was run to find the best χ^2-fit. The full lines in Fig. 2 and Fig. 3(a) show typical fits to the spectra collected during irradiation. For spectra which were collected long after the irradiation, and consequently had one or two very well separated α-lines, the intensities were obtained by simple peak integration. The resulting intensities were then corrected for dead times, prior to obtaining the cross sections for individual channels (see Sec. V).

IV. IDENTIFICATION OF THE REACTION PRODUCTS

The main peaks in the α-particle spectra for the ^{6,7}Li induced reactions are from Rn,At,Po isotopes (see Fig. 3), and for the ^{9}Be case from Rn and Po (see Fig. 2). The Rn nuclei result from neutron-evaporation from the compound nucleus formed following complete fusion of the projectile with the target. The At and Po nuclei can result from α-decay, electron capture and/or β^+ decay of Rn nuclei, as shown in Fig. 4 for the ^{211}Rn decay chain. However, the measured cross sections for At and Po were well in excess of those calculated from the measured decay of the Rn isotopes, indicating that there is another mechanism populating these nuclei directly.

A. Origin of the At and Po nuclei

Complete fusion followed by αxn and *xnyp* evaporation could, in principle, lead to Po and At residual nuclei. However, for the ^{9}Be+^{208}Pb system, prompt α-particles measured in coincidence with gamma transitions in Po nuclei showed angular distributions inconsistent with fusion evaporation [23,24]. The origin of the yields of these nuclei was investigated by the measurement of above-barrier fusion cross sections for the ^{18}O+^{198}Pt [25] and ^{13}C+^{204}Hg reactions, that form the same compound nuclei as ^{7}Li+^{209}Bi and ^{9}Be +^{208}Pb, respectively, at similar excitation energies. The production cross sections of Po and At nuclei for the ^{18}O and ^{13}C induced reactions were found to be insignificant ($<$2% of σ_{xn}) at all measured energies (excitation energy $>$35 MeV). Therefore, the direct production of Po and At observed for the reactions induced by ^{6,7}Li and ^{9}Be projectiles cannot be due to CF.

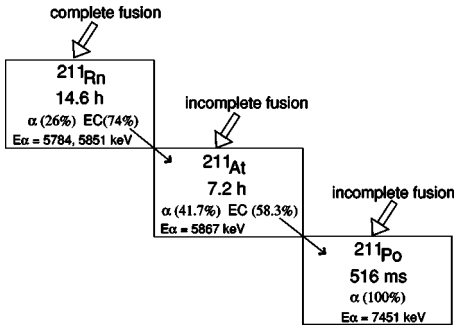

FIG. 4. The decay of the ^{211}Rn nucleus by EC and/or β^+ to ^{211}At and ^{211}Po nuclei. The wide arrows indicate direct population by complete and incomplete fusion.

The breakup of the projectile into two charged fragments provides a mechanism for the direct production of Po and At isotopes. The breakup of ^{6}Li into ^{4}He and ^{2}H followed by absorption of one of these fragments by ^{209}Bi will lead to the formation of ^{213}At and ^{211}Po. Subsequent evaporation of neutrons from these nuclei will give rise to various isotopes of At and Po, as observed experimentally. Similarly, incomplete fusion for ^{7}Li will lead to ^{213}At and ^{212}Po, while that for ^{9}Be will lead to the nuclei ^{212}Po and ^{213}Po. The Po and At nuclei were therefore attributed to ICF, where following breakup of the projectile, just one of the charged fragments fuses with the target (fusion of both fragments with the target leads to the same product as CF). Transfer reactions that produce these nuclei may in principle be present. A recent study of ^{9}Be+^{208}Pb [26] has found large yields of α-particles at subbarrier energies. One component had a broad energy spectrum, consistent with prompt breakup, while the other clearly resulted from breakup of the ^{9}Be$_{g.s.}$, associated with neutron stripping and Coulomb excitation of ^{9}Be. No contribution from α-particle transfer to discrete states could be identified. Thus transfer contributions are expected to be small for the reactions studied in this work.

B. Other reaction products

In the ^{7}Li induced reaction, small yields ($\sim$10 mb at the highest energy) of the nucleus ^{211}Bi were observed (see Table VII later). This is likely to be due to two neutron transfer from the projectile to the target with a *Q*-value of $-$3.17 MeV. Apart from Po and At nuclei which can be populated by transfer, ^{211}Bi is the only other transfer product which is alpha active with a short enough lifetime to be observed in the present experiments. In the ^{6}Li reactions, the *Q*-value for two neutron stripping is $-$17.44 MeV, thus making the transfer process much less likely than in the case of ^{7}Li.

V. DETERMINATION OF CROSS SECTIONS FROM α-DECAY MEASUREMENTS

The determination of production cross sections of individual nuclei from the α-decay measurements requires the

knowledge of (a) the detector solid angle, (b) the product of the number of incident beam particles and target atoms for normalization, and (c) the total number of nuclei produced, for which the alpha branching ratios and the interplay of α-decay lifetimes and data collection times must be accounted for. The normalization and solid angle measurements have been discussed in Secs. II and III, respectively. The number of nuclei produced can be determined from the known α-yields, lifetimes, branching ratios, irradiation time, collection time, dead time, and production and decay formulae which can be simply derived. For the evaporation channels giving residues with half lives much smaller than the irradiation times of typically 0.5−1.0 hour, e.g., $T_{1/2} \leqslant$ a few minutes, saturation activity is reached, and the formula for determining the cross sections is even simpler. The determination of cross sections for the ^{211}Rn and ^{211}At nuclei was more involved and is discussed here briefly.

For the Li induced reactions, ^{211}At is populated from the parent nucleus ^{211}Rn by electron capture (EC) decay, but is also directly populated by ICF (see Fig. 4). Both the nuclei ultimately decay by EC to ^{211}Po, which is also directly populated by ICF in the three reactions studied here. The α-decay energies could not be used in the present experiment for determining the individual cross sections since the decay α energies for ^{211}Rn (5783.9 keV and 5852.2 keV) are too close to that of the ^{211}At (5869.5 keV). The differences in their half lives were therefore exploited in determining their yields. The half life of the parent nucleus ^{211}Rn is 14.6 h, while the half life of the EC-decay daughter ^{211}At is 7.2 h, and that of the EC-decay grand-daughter ^{211}Po(g.s.) is shorter still being only 0.516 s. The time evolution of the intensity of the 7451 keV decay α from ^{211}Po(g.s.), which is energetically well separated from those from ^{211}Rn and ^{211}At, was used for cross section determination. The direct population of ^{211}Po(g.s.) was obtained from the 7451 keV peak in the spectrum collected during irradiation, making a small correction for feeding due to decay. The same measurement was also used to determine the population of the ^{211}Po isomeric state [spin=$(25^{+}/2)T_{1/2}$=25.2 s] which is not fed by the decay of Rn or At. The cross sections for direct population of ^{211}Rn and ^{211}At were determined individually from two separate off-line measurements: one was made soon after the end of irradiation where the counts in the 7451 keV peak are mainly due to the decay of ^{211}At, while the other was made typically 30 h after the end of irradiation, where feeding from the decay of ^{211}Rn is dominant. The individual cross sections for ^{211}Rn and ^{211}At could then be obtained from the above measurements by solving two simultaneous radioactive decay equations. In the case of the ^{9}Be induced reaction, there is no direct population of ^{211}At, making it simpler to determine the cross section of ^{211}Rn from the 7451 keV offline α-yield.

VI. COMPLETE FUSION RESULTS

It was shown in Sec. IV that amongst the observed evaporation residues, only Rn isotopes are the result of complete fusion of the projectile with the target. Rn isotopes will also be produced if both the charged breakup fragments are captured by the target (thus technically breakup), and also if ^{9}Be breaks up into a neutron and ^{8}Be (Q=−1.67 MeV) and the latter is captured by the target. Likewise for the Li induced reactions, our experimental definition of complete fusion includes the capture of ^{5}Li and ^{6}Li. However, the probability of ^{6}Li (^{7}Li) breaking up into ^{5}Li (^{6}Li) and a neutron may be expected to be much smaller than that for $^{9}\mathrm{Be} \rightarrow n + {}^{8}\mathrm{Be}$, due to the large negative Q-values for breakup into these partitions (−5.67 MeV for ^{6}Li and −7.25 MeV for ^{7}Li).

The observed fission cross sections were attributed to CF, since fission following ICF is expected to be negligible due

TABLE II. Complete fusion cross sections and the cross sections for individual evaporation residues and fission components following the fusion of ^{6}Li with ^{209}Bi. The $E_{\mathrm{c.m.}}$ is corrected for energy losses in the target.

E_{beam} (MeV)	$E_{\mathrm{c.m.}}$ (MeV)	$\sigma_{2n}(^{213}\mathrm{Rn})$ (mb)	$\sigma_{3n}(^{212}\mathrm{Rn})$ (mb)	$\sigma_{4n}(^{211}\mathrm{Rn})$ (mb)	$\sigma_{5n}(^{210}\mathrm{Rn})$ (mb)	$\sigma_{\mathrm{fission}}$ (mb)	σ_{CF} (mb)
26.00	25.13	0.10±0.07[a]	0.33±0.16				0.43±0.17
27.00	26.16	0.34±0.14	1.12±0.38			0.002±0.001	1.46±0.40
28.00	27.11	0.63±0.13	4.7±0.6			0.008±0.002	5.3±0.6
29.00	28.06	1.00±0.12	15.1±0.8			0.040±0.003	16.1±0.8
30.00	29.08	1.48±0.18	36.1±1.3			0.137±0.008	37.7±1.3
31.00	30.04	1.82±0.20	66.0±4.0			0.350±0.002	68.2±4.0
32.00	30.98	2.38±0.22	105.5±1.7	4.6±0.8		0.80±0.01	113.3±1.9
33.00	32.00	1.99±0.24	149.8±2.5	15.2±1.5		1.48±0.02	168.5±2.9
34.00	32.96		175.2±4.0	48.0±2.0		2.58±0.03	225.8±4.5
36.00	34.92		176.1±2.5	162.7±3.7		5.90±0.03	344.7±4.5
38.00	36.86		131.3±2.4	309±8		11.03±0.05	451±8
40.00	38.81		91.2±3.0	445±18	3.7±0.7	18.4±0.4	558±18
44.00	42.70		39.5±0.7	530±58	95.4±2.4	37.8±0.5[b]	703±58
48.00	46.58		24.4±0.5	394±17	412±3	65.3±1.1	896±18

[a]Extrapolated value.
[b]Interpolated value.

TABLE III. Complete fusion cross sections and the cross sections for individual evaporation residues and fission components following the fusion of ^{7}Li with ^{209}Bi. The $E_{\mathrm{c.m.}}$ is corrected for energy losses in the target.

E_{beam} (MeV)	$E_{\mathrm{c.m.}}$ (MeV)	$\sigma_{2n}(^{214}\mathrm{Rn})$ (mb)	$\sigma_{3n}(^{213}\mathrm{Rn})$ (mb)	$\sigma_{4n}(^{212}\mathrm{Rn})$ (mb)	$\sigma_{5n}(^{211}\mathrm{Rn})$ (mb)	$\sigma_{\mathrm{fission}}$ (mb)	σ_{CF} (mb)
26.00	25.02	0.18±0.06	0.12±0.05				0.30±0.08
27.00	26.01	0.71±0.13	0.75±0.11				1.46±0.17
28.00	26.98	1.36±0.16	3.94±0.24			0.006±0.001	5.31±0.29
29.00	27.95	2.31±0.71	14.3±0.4			0.023±0.002	16.6±0.8
30.00	28.92	3.10±0.95	39.0±0.8			0.079±0.003	42.2±1.2
31.00	29.89	2.50±0.53	79.3±0.3	1.70±0.36		0.230±0.006	83.7±0.7
32.00	30.86	1.20±0.61	126.4±2.1	9.3±1.8		0.59±0.01	137.5±2.8
33.00	31.77	1.1±0.6[a]	173.2±4.0	38.7±2.5		1.08±0.04[a]	214.1±4.8
33.00	31.83	1.04±0.53	171.1±2.8	33.3±2.6		1.13±0.02	206.6±3.9
34.00	32.80		192.4±3.1	80.9±3.6		1.99±0.02	275.3±4.8
35.00	33.70		193.1±5.4	165.3±5.5		3.0±0.1[a]	361.4±7.7
35.00	33.77		195.0±3.2	154.3±4.9		3.16±0.03	352.5±5.9
36.00	34.70		184.1±4.3	243.7±7.9		4.48±0.04	432.3±9.0
37.00	35.50		155.3±3.9	326.8±7.1		6.0±0.3[a]	488.1±8.1
38.02	36.68		126.9±3.6	407.8±6.5		9.0±0.1	543.7±7.4
39.00	37.59		106.0±5.2	528±14		11.7±0.7[a]	646±15
40.00	38.63		82.9±2.2	567±13	8.2±1.0	15.0±0.1	673±13
44.00	42.53		37.3±1.7	665±16	129±8	32.7±0.2	864±18
48.00	46.34		19.6±1.6	433±11	513±35	59±1[a]	1025±37
48.00	46.38	$\sigma_{6n}(^{210}\mathrm{Rn})$	21.0±1.1	426.4±8.4	495±14	59.4±0.3	1002±16
52.00	50.23	34.0±4.0	12.5±0.5	222.5±5.5	769±46	95.3±0.5	1133±47

[a]Interpolated value.

to the lower angular momentum and excitation energy brought in, and the higher fission barriers of the resulting (lower Z) compound nuclei. The measured cross sections for each Rn isotope, and for fission, for the ^{6}Li+^{209}Bi, ^{7}Li +^{209}Bi, and ^{9}Be+^{208}Pb systems, are given in Tables II–IV, and shown in Figs. 5–7 as a function of the center of mass energy $E_{\mathrm{c.m.}}$. The beam energy loss in the target has been accounted for, hence beams of identical energy incident on targets with different thicknesses (in different runs) result in different $E_{\mathrm{c.m.}}$. The measured cross sections for ^{6}Li+^{209}Bi and ^{7}Li+^{209}Bi are in good agreement with those of Ref. [27], which cover the energy range $E_{\mathrm{c.m.}} \simeq 24$ to 33 MeV.

Cross sections for each xn-channel for all three systems, presented in Figs. 5–7, show a gradual rise and fall with energy as expected. This is seen more clearly by plotting the ratio of the yield of a given xn channel to the total xn cross section as a function of the excitation energy E^{*} of the compound nucleus. The measured ratios are shown in Figs. 8(a) and 8(b) for the ^{7}Li+^{209}Bi and ^{9}Be+^{208}Pb reactions, the dashed lines being presented to guide the eye. The increase in the width of the xn-distribution with an increasing number of evaporated neutrons is expected, as evaporation causes a spread in the excitation energy of the residual nucleus. However, the distribution for the 4n evaporation channel for the ^{7}Li+^{209}Bi case is much wider than the 4n channel for ^{9}Be +^{208}Pb. This may be because 4n evaporation in ^{7}Li leads to the closed neutron shell nucleus ^{212}Rn (N=126), making 4n evaporation more favorable than 3n- or 5n-evaporation. A similar situation arises for ^{6}Li+^{209}Bi (not shown) where the width of the 3n channel is larger, while for ^{9}Be+^{208}Pb the 5n channel is expected to be wider.

The relative xn yields are compared with those measured for ^{18}O+^{198}Pt [Fig. 8(c)] and ^{13}C+^{204}Hg [Fig. 8(d)] which form the same compound nucleus as the ^{7}Li and ^{9}Be induced reactions, respectively. For these reactions the fusion barrier energies and Q-values are such that the lowest energy at which the measurements could be made corresponds to $E^{*} \sim 35$ MeV. Thus the overlap the with ^{7}Li and ^{9}Be induced reactions is only in a narrow energy range. A better comparison can be made using the mean neutron multiplicity, as it can be determined from the data with small uncertainties, and importantly it is expected to vary approximately linearly over a wide energy range [28]. Figure 9 shows this quantity as a function of E^{*} for the ^{7}Li+^{209}Bi and ^{18}O+^{198}Pt systems in panel (a), and for the ^{9}Be+^{208}Pb and ^{13}C+^{204}Hg reactions in the panel (b). The dashed lines are to guide the eye. The small oscillations about the straight line are expected and can be most easily understood by taking the limit of zero kinetic energy of the evaporated neutrons, and fixed compound nucleus angular momentum. In this case the mean multiplicity as a function of E^{*} would look like a staircase, with each step corresponding to the E^{*} at which the emission of another neutron becomes energetically possible. The finite kinetic energy carried by the neutrons and the spread in compound nucleus angular momentum washes out the structure, which ultimately disappears at high energies.

TABLE IV. Complete fusion cross sections and the cross sections for individual evaporation residues and fission components following the fusion of ^{9}Be with ^{208}Pb. The $E_{c.m.}$ is corrected for energy losses in the target.

E_{beam} (MeV)	$E_{c.m.}$ (MeV)	$\sigma_{2n}(^{215}Rn)$ (mb)	$\sigma_{3n}(^{214}Rn)$ (mb)	$\sigma_{4n}(^{213}Rn)$ (mb)	$\sigma_{5n}(^{212}Rn)$ (mb)	$\sigma_{fission}$ (mb)	σ_{CF} (mb)
36.00	34.40	0.35±0.19	0.21±0.11			0.0002±0.0001	0.56±0.22
37.00	35.37	1.45±0.40	1.34±0.17			0.0016±0.0005	2.79±0.43
38.00	36.33	2.01±0.63	7.5±0.7			0.0061±0.0015	9.5±0.9
39.00	37.29	1.86±0.92	21.8±1.4			0.0294±0.0040	23.7±1.7
40.00	38.25	3.40±0.76	52.1±2.0			0.083±0.006	55.6±2.1
41.02	39.22	2.72±0.71	86.1±2.7	2.74±0.49		0.250±0.016	91.8±2.8
42.00	40.16	4.90±1.08	124.3±3.7	12.8±1.1		0.468±0.020	142.5±4.0
43.00	41.12	3.17±1.06	147.3±4.6	34.52±2.33		0.888±0.031	185.9±5.3
44.06	42.15		162.9±4.2	79.3±2.6		1.46±0.03	243.7±4.9
45.00	43.05		162.4±4.6	138.6±4.6		2.14±0.04	303.1±6.5
46.00	44.01		139.1±4.1	207.7±5.0	1.5±0.5[a]	3.13±0.04	351.4±6.6
47.00	44.96		108.9±3.4	286.6±6.9	3.6±0.5[a]	4.45±0.05	403.6±7.7
48.00	45.92		84.4±2.8	355.8±8.1	7.8±0.8	5.85±0.06	453.8±8.6
49.00	46.88		64.8±2.6	419.5±9.5	15±2[b]	7.90±0.06	507±10
50.00	47.84		50.6±2.1	479±11	30±3[b]	10.31±0.07	570±12
51.00	48.80		35.8±2.1	488±11	57±4	12.80±0.09	594±12

[a]Extrapolated value.
[b]Interpolated value.

It is clear from Fig. 9 that the data for the lighter projectiles are shifted towards higher energies. An energy shift of −1.7 MeV for ^{7}Li and −1.3 MeV for ^{9}Be brings them in agreement with their heavier counterparts. The energy offset could be due to two effects. Firstly, pre-equilibrium emission for the lighter projectiles may be present due to the higher beam velocity (i.e., larger energy per nucleon) at the same excitation energy, leading to lower multiplicities. The velocities of ^{7}Li and ^{9}Be are, respectively, 22% and 8% higher than that of the ^{18}O and ^{13}C projectiles. Second, the average angular momenta of the compound nuclei formed by the lighter projectiles are higher than those for the heavier projectiles. For instance, at $E^{*}=40$ MeV, the predicted average angular momenta of the CN ^{216}Rn formed by ^{7}Li and ^{18}O projectiles are $\simeq 16\hbar$ and $12\hbar$, respectively, while for ^{217}Rn formed by ^{9}Be and ^{13}C projectiles they are $\simeq 19\hbar$ and $16\hbar$, respectively. This means that at the same excitation energy, the available energy above the yrast line is lower for the lighter projectiles, resulting in lower multiplicities. In the case of ^{9}Be, the observed energy shift could also result from ICF with ^{8}Be. The presence of incomplete fusion is likely to affect the angular momentum distribution for complete fusion making quantitative calculations unreliable until the incomplete fusion process is better understood. The dashed curves in Figs.

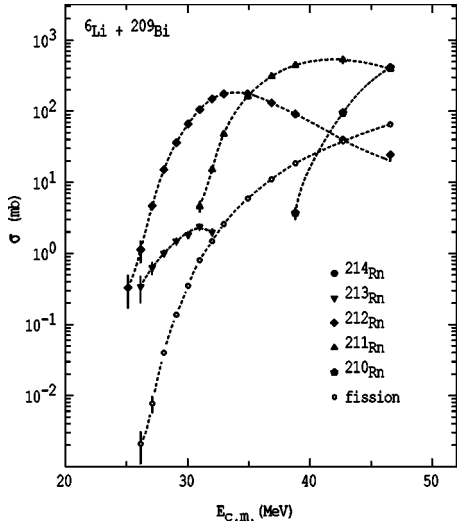

FIG. 5. Excitation functions for *xn*-channels and fission for the ^{6}Li+^{209}Bi system. The dashed lines serve to guide the eye.

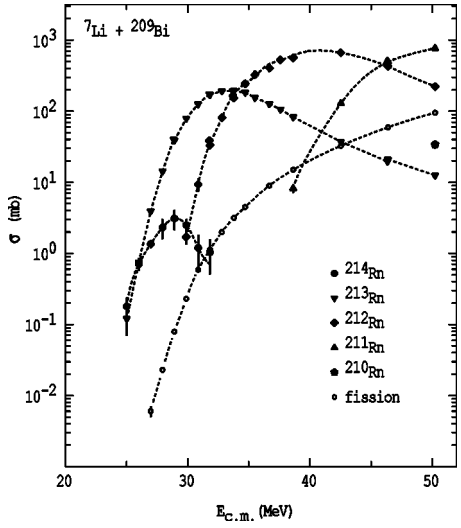

FIG. 6. Excitation functions for *xn*-channels and fission for the ^{7}Li+^{209}Bi system. The dashed lines guide the eye.

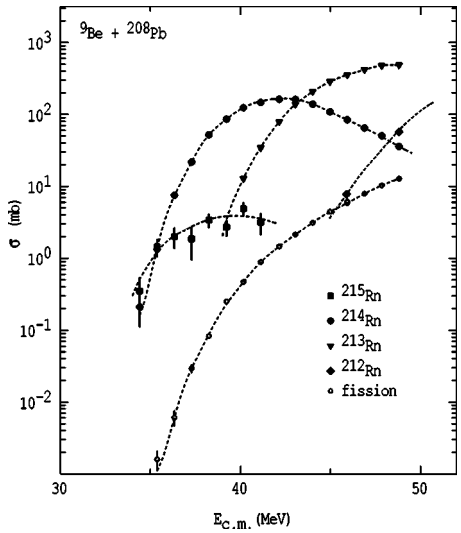

FIG. 7. Excitation functions for *xn*-channels and fission for the ^{9}Be+^{208}Pb system. The dashed lines guide the eye.

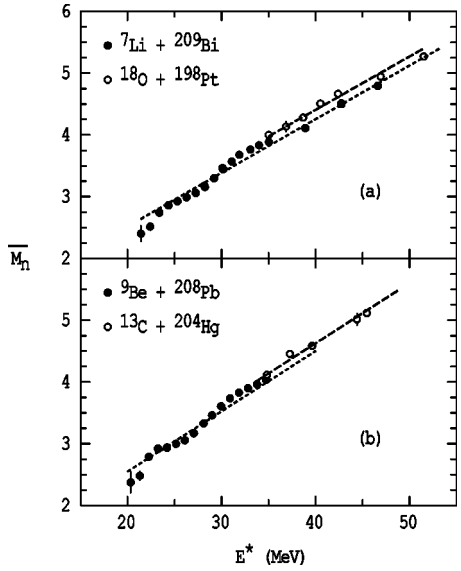

FIG. 9. The average neutron multiplicities as a function of compound nucleus excitation energy for the two sets of reactions (a) ^{7}Li+^{209}Bi and ^{18}O+^{198}Pt and (b) ^{9}Be+^{208}Pb and ^{12}C+^{204}Hg, which form the compound nuclei ^{216}Rn and ^{217}Rn, respectively. The dashed lines guide the eye.

8(a) and 8(b), which describe the data for the ^{7}Li and ^{9}Be induced reactions, when shifted by −1.7 MeV and −1.3 MeV, respectively (full lines in Fig. 8, top panels), describe well the data for ^{18}O+^{198}Pt and ^{13}C+^{204}Hg, respectively, as shown by the full lines in the corresponding bottom panels of Fig. 8. This demonstrates that the individual *xn* channels as well as the mean multiplicity behave in a very similar way for the different reactions.

A. The cross sections and barrier distributions for complete fusion

The total complete fusion cross sections, obtained by summing the cross sections for the Rn isotopes and the fission cross sections, are given in the last column of Tables II–IV, and are plotted in Figs. 10(a), 11(a), and 12(a) for the ^{6}Li+^{209}Bi, ^{7}Li+^{209}Bi, and ^{9}Be+^{208}Pb systems, respectively. The experimental barrier distributions, evaluated by taking the second derivative of the quantity $E_{c.m.}\sigma_{fus}$ with respect to the energy $E_{c.m.}$ using a point difference formula [29], are shown in Figs. 10(b), 11(b), and 12(b). For the Li induced reactions a step length of ≈2 MeV was used for energies $E_{c.m.} \leqslant 37$ MeV, and of 3.5 MeV for higher energies. For ^{9}Be a step length of 1.92 MeV was used at all energies. The ability to determine the experimental distribution of barriers proved to be very important, as the centroids of these distributions were used to constrain the theoretical calculations, enabling the quantitative determination of fusion suppressions. The shape of the barrier distribution provides an indication of the importance of the couplings involved. The low charge products ($Z_P Z_T$) of the projectile and target combinations, however, means that the couplings are not as strong as in the case of reactions with heavier projectiles. This is reflected in the narrow, almost structure-less distributions for all three reactions.

B. Determination of the average barrier energy

The average barrier energy is often determined experimentally by fitting the high energy data with a single barrier

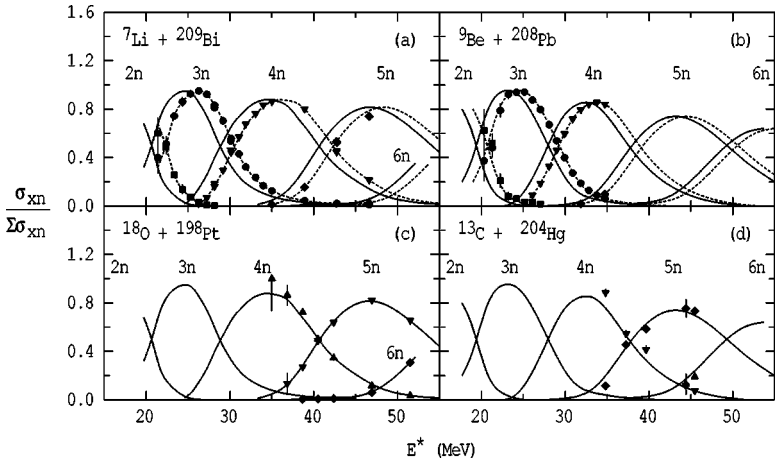

FIG. 8. A comparison of the proportion of individual *xn*-channels for two different sets of reactions, with each set [(a) and (c); (b) and (d)] forming the same compound nucleus. The dashed lines in panel (a) and (b) guide the eye. The full lines in panels (a) and (b) are obtained by shifting the dashed curves by 1.7 MeV and 1.3 MeV. These shifted curves are reproduced in panel (c) and (d) and describe well the data for the ^{18}O +^{198}Pt and ^{12}C+^{204}Hg reactions.

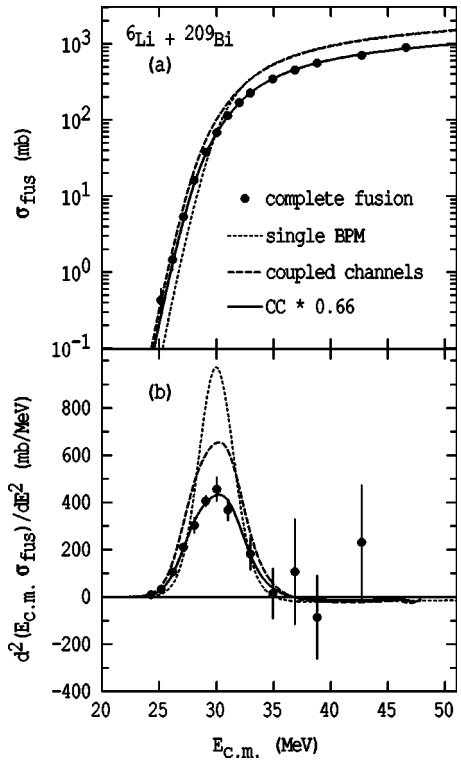

FIG. 10. The measured and calculated (a) complete fusion excitation function and (b) experimental barrier distribution for the fusion of ^{6}Li with ^{209}Bi. The short-dashed lines are the predictions of a single barrier penetration model, and the long dashed lines are the results of a coupled channels calculation (see the text). The full line is the latter calculation multiplied by the indicted factor.

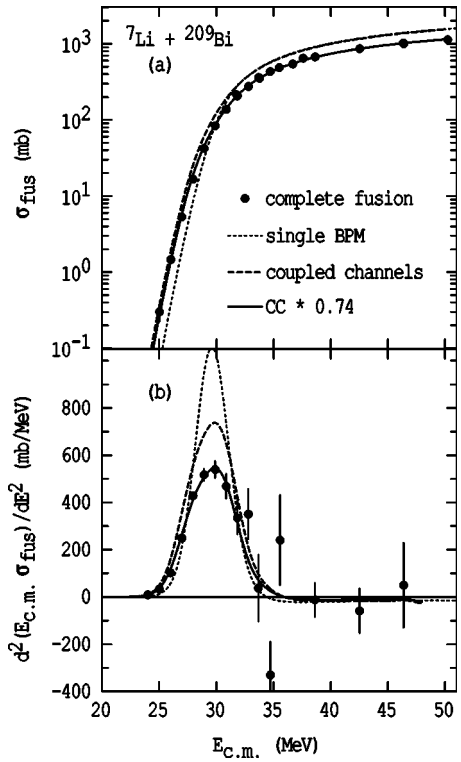

FIG. 11. The measured and calculated (a) complete fusion excitation function and (b) experimental barrier distribution for the fusion of ^{7}Li with ^{209}Bi. The lines have the same meaning as in Fig. 10.

penetration (SBP) calculation using the approximate relationship $\sigma_{\rm fus} \simeq \pi R^2(1-B_0/E_{\rm c.m.})$. Here B_0 is the $\ell=0$ barrier used in the SBP calculations, which is taken to be equal to the average barrier. R is the fusion barrier radius which is often assumed to be constant and equal to R_0, but in reality is a slowly varying function of ℓ and hence energy. However, this prescription of fitting high energy data may not be applicable in these reactions, as the suppression of fusion due to breakup may be energy dependent. If the average barrier energy is instead determined from the centroid of the experimental barrier distribution, then data from only a narrow energy range of $E \simeq B_0$ is used and, furthermore, it can be shown [29] that a linear energy dependence of suppression does not affect the determination of the centroid. The centroid of the experimental barrier distribution is close, but not equal to B_0, because of the slow decrease in R with increasing energy [this gives rise to the negative values of $d^2(E_{\rm c.m.}\sigma_{\rm fus})/dE^2$ at higher energies seen most clearly for the single barrier penetration calculations in Figs. 10(b), 11(a), 11(b), 12(a), and 12(b). For example for ^{6}Li+^{209}Bi the centroid of the barrier distribution for a single barrier penetration calculation using $B_0=30.1$ MeV is 30.0 MeV, i.e., there is a 0.1 MeV shift between the centroid and B_0 used in the SBP calculations. The shift is not of any consequence (except when quoting B_0), since the calculations presented here for the three systems were performed by matching the centroids of the calculated barrier distribution to that of the experimental barrier distribution. The following steps were taken to determine the centroid of the experimental barrier distribution and its uncertainty: (i) the measured fusion cross sections were randomly scattered from their measured values with Gaussian distributions of standard deviation equal to those of the experimental uncertainties, (ii) a barrier distribution was determined from these data using a point difference formula, (iii) this barrier distribution was used to calculate the centroid. Steps (i)–(iii) were repeated many times with different random scatter, to generate a frequency distribution for the centroid energy. The mean value and the variance of this frequency distribution gave the centroid and its uncertainty. The distributions in step (ii) were calculated with all energy steps between 1.7 MeV to 4.0 MeV for the ^{6}Li reaction, 1.9 to 4.0 MeV for the ^{7}Li induced reaction and 1.8 MeV to 4.0 MeV for the ^{9}Be reaction.

The centroid depends upon the energy range of the data used in determining it. This dependence is illustrated in Fig. 13 where the centroids for ^{6}Li and ^{7}Li are plotted against the upper energy cut imposed on their respective experimental barrier distributions. If data points only from the first half of the barrier distributions are included, then the corresponding centroid is low, as expected. The most representative value of the centroid is obtained at the energy where the barrier distribution returns close to zero. Beyond this energy, the uncertainty in the centroid increases, reflecting the increased uncertainty in the determination of the barrier distribution. The centroids determined by using the barrier distributions from only a narrow range of energy steps, corresponding to

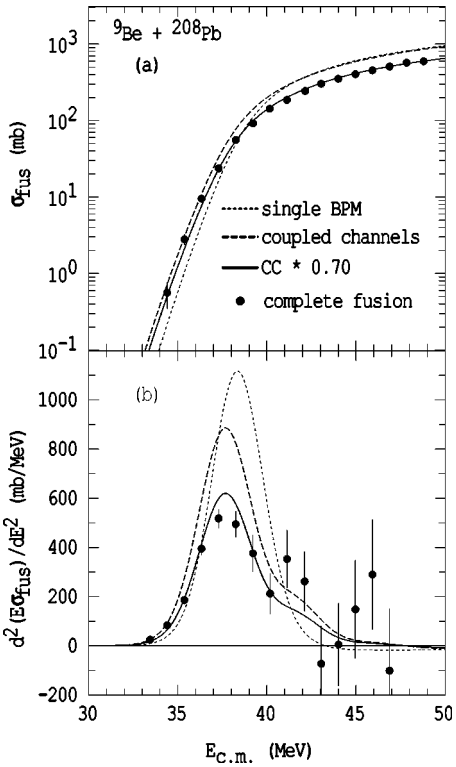

FIG. 12. The measured and calculated (a) complete fusion excitation function and (b) experimental barrier distribution for the fusion of ^{9}Be with ^{208}Pb. The lines have the same meaning as in Fig. 10.

those in Figs. 13(a) and 13(b), are also shown in the corresponding bottom panels by the filled circle and the hollow square, and match those determined with a larger range in step lengths. The full horizontal line indicates the adopted centroid position and the dotted lines the adopted uncertainty. The energies of the centroids obtained from the experimental barrier distributions are 30.0±0.3 MeV (corresponding to B_0 of 30.1 MeV), 29.6±0.2 MeV (B_0 =29.7 MeV), and 38.2±0.6 MeV (B_0=38.3 MeV), for the ^{6}Li+^{209}Bi, ^{7}Li+^{209}Bi, and ^{9}Be+^{208}Pb systems, respectively.

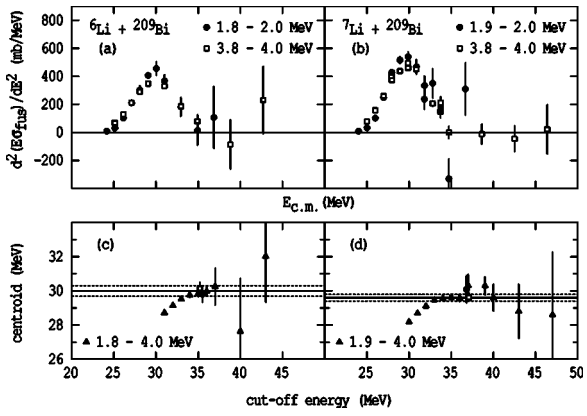

FIG. 13. The upper panels show the experimental fusion barrier distributions for the reactions ^{6}Li with ^{209}Bi (a) and ^{7}Li with ^{209}Bi (b), determined using center of mass step lengths as indicated. The bottom panels show the variation of the centroid position with upper energy cut imposed on the barrier distribution data. The solid line shows the adopted centroid position, and the dashed lines the adopted uncertainty.

VII. COMPARISON WITH THEORETICAL MODELS

Modelling the effect of breakup on fusion requires modelling of the complete dynamics, including (*i*) couplings to bound and continuum states (*ii*) an appropriate coordinate system to describe the physical boundary condition for the wave-functions of the breakup fragments, and (*iii*) modelling of the trajectories of the breakup fragments to determine whether one or both fragments are captured by the target nucleus. The first of these points has led to controversies in the past, with some authors predicting enhancement due to couplings to unbound and continuum states (sometimes referred to in the literature as breakup states) while some others predicted a reduction in fusion due to loss of flux resulting from breakup. These two opposing views were reconciled in Ref. [14], where it was shown that in fact there are two effects of couplings leading to continuum states: (1) the enhancement of complete fusion at energies below the average barrier (as in the familiar case of stable nuclei), and (2) reduction in flux in the bound channels due to breakup of the projectile before reaching the fusion barrier. Similar conclusions were also arrived at in Ref. [15], where continuum-continuum couplings were also included. In the continuum discretized coupled channels (CDCC) calculations such as those of Refs. [14,15], complete fusion is defined as absorption from the bound states, and incomplete fusion as absorption from the unbound states. The calculations thus provide only an upper limit to the reduction in fusion, since the possibility [9] that following breakup, all the fragments could subsequently fuse with the target nucleus is not accounted for. Thus, quantitative predictions of the complete-fusion cross sections and barrier distribution using the CDCC model requires a good understanding of the couplings to unbound states and also a prescription to follow the breakup fragments. Since this has not yet been achieved, and because of the time consuming nature of the CDCC calculations, we do not attempt such calculations here.

The experimental cross sections and barrier distributions are instead compared with expectations of the single barrier penetration model and coupled channel calculations which do not consider couplings to unbound or continuum states. Thus, breakup of the projectile is not included. The calculations are presented here to demonstrate that, at above-barrier energies, complete fusion is suppressed for nuclei which breakup at low excitation energies compared to those which do not. This is obtained on the basis of *only one* constraint—that the centroid of the calculated fusion barrier distribution matches that obtained from the measurement. The single barrier penetration (SBP) calculations and the coupled channels calculations were performed using the code CCFULL [30]. This code solves the Schrödinger equation and the coupled equations exactly, making only the iso-centrifugal approximation. The fusion cross sections are calculated using an incoming wave boundary condition. The nuclear potential was taken to be of a Woods-Saxon form. The depth V_0 and

radius parameter r_0 used for the single barrier penetration calculations for the ^{6}Li+^{209}Bi, ^{7}Li+^{209}Bi, and ^{9}Be+^{208}Pb systems, were V_0=107 MeV, r_0=1.12 fm, V_0=113 MeV, r_0 =1.12 fm, and V_0=198.00 MeV, r_0=1.10 fm, respectively. The values of V_0 and r_0 were chosen such that the centroids of the calculated fusion barrier distributions for each system matched those measured. Also with these values of V_0 the CCFULL calculations could be carried out successfully at all measured $E_{\mathrm{c.m.}}$. Choosing a small value of V_0 causes the potential pocket to disappears at larger values of angular momenta and fusion can no longer be defined [31] in CCFULL. The diffuseness parameter a of the Woods-Saxon nuclear potential was initially set to 0.63 fm for all three reactions. This value is very close to the predictions using the Woods-Saxon parametrization [32] of the Akyüz-Winther potential [33] which gives a=0.62 fm, 0.63 fm and 0.64 fm, respectively, for the ^{6}Li, ^{7}Li, and ^{9}Be induced reactions. The effect on the fusion suppression factor of varying the diffuseness parameter is shown to be small, as discussed in Sec. VIII C. For calculations including couplings (see Sec. VII B) the depth V_0 had to be changed slightly, since the introduction of couplings changes the average barrier energy slightly. The analyses of the complete fusion excitation functions have already been reported [6,9], and in the following only a brief description of them will be given. The suppression factors and the variables affecting them are however discussed in more detail here.

A. Single barrier penetration model

The results of the SBP calculations (dotted lines) are compared with the measured complete fusion cross sections in the upper panels of Figs. 10–12, and with the barrier distributions in the lower panels. The calculations underestimate the measured cross sections at energies below the barrier by a factor of $\sim$5 for Li reactions and slightly more for the Be reaction. The underestimate is not unexpected, resulting from neglect of couplings between the relative motion and the intrinsic states (bound and unbound) of the projectile and target. For larger values of $Z_P Z_T$ this enhancement is found to be 2–3 orders of magnitude, but in the present systems the enhancement is much smaller due to their low $Z_P Z_T$ values. However, at above-barrier energies in all three reactions studied here, the measured cross sections lie below the predictions. Using the data above $E_{\mathrm{c.m.}}$=36 MeV, for ^{6}Li and ^{7}Li, they are, respectively, 65^{+5}_{-4}% and 73^{+3}_{-2}% of the SBP predictions. The quoted uncertainties include the contributions from both statistical and measured uncertainty in the energy of the centroid, with the latter being the main contributor (see Sec. VIII B). For the case of ^{9}Be the percentage reduction is 0.68^{+8}_{-7}% using the data above 44 MeV.

B. Coupled channels calculations

The lowest collective states of the target nuclei were included in the CCFULL calculations. For ^{209}Bi, the septuplet and decuplet of identified states [34] associated with the 3^- and 5^- collective excitations, respectively, were each approximated [34] by a single level with an energy equal to that of the centroid of each multiplet and a deformation length corresponding to that of the combined states [34]. These states and the double octupole phonon state were included in the CCFULL calculations. For ^{208}Pb, the collective 3^- and 5^- states and double octupole phonons states were included in the harmonic limit. Since the calculations presented here do not include the couplings to the unbound and continuum states in the projectile (see discussions in Sec. VII), the couplings to the included projectile states were adjusted to reproduce the shape of the measured barrier distributions. A reasonable reproduction of the shape for the Li induced reactions could be obtained by including rotational couplings with β_2 deformation parameters of 0.87 and 0.80 for ^{6}Li and ^{7}Li, respectively. Here couplings were considered only to the first rotational state, which was taken to be degenerate with the ground state. The nuclei ^{6,7}Li are not good rotors and hence the coupling scheme is probably unrealistic, but is only used here to obtain a reasonable fit. In the reaction with ^{9}Be, couplings to the $\frac{5}{2}^-$ and $\frac{7}{2}^-$ states in the $K^\pi = \frac{3}{2}^-$ ground state rotational band with a β_2 of 0.92 were included. The dashed curves in Figs. 10–12 show the predictions of the CCFULL code for the ^{6}Li+^{209}Bi, ^{7}Li+^{209}Bi, and ^{9}Be+^{208}Pb systems. While the calculated cross sections below the barrier are somewhat higher than those measured, the calculations above the barrier are consistently well above the measured cross sections, and are almost identical to the SBP calculations, as expected. The measured CF cross sections are thus suppressed at above barrier energies due to breakup. This also appears to be the case at sub-barrier energies, but the suppression cannot be reliably determined in the presence of the couplings that enhance the CF cross sections, since as discussed above the couplings are not yet sufficiently well understood.

VIII. COMPLETE FUSION SUPPRESSION FACTORS

The measured cross sections at above-barrier energies are 66^{+5}_{-4}%, 74^{+3}_{-2}%, and 70^{+8}_{-7}% of the coupled channels predictions for the ^{6}Li+^{209}Bi, ^{7}Li+^{209}Bi, and ^{9}Be+^{208}Pb, respectively. The uncertainties include statistical uncertainties, but arise mainly from the experimental uncertainties in the energy of the centroid as discussed in Sec. VIII B. The latter does not affect the relative suppression of ^{6}Li to ^{7}Li, which is determined to be 0.89 ± 0.02 by taking the ratios of the measured cross sections since the small differences in the calculated high energy cross sections due to difference in their barrier energies is negligible.

As discussed in the introduction to Sec. VI, the CF cross sections may include those incomplete-fusion events where all the charge of the projectile is captured, e.g., capture of ^{8}Be by the target. It may be argued that since the final products are so similar that a distinction cannot be made experimentally, it does not matter whether it results from complete or incomplete fusion. This is true if the interest is only in the population of a particular nucleus. However, if the aim is to understand the reaction mechanism then this distinction becomes important. For example, large breakup and transfer probabilities [35] in reactions with radioactive beams may lead to significant incomplete fusion or transfer events which look like complete fusion. If all these events were taken to be

"true" complete fusion, then it could easily lead to wrong conclusions about the fusion process. In the present work if incomplete fusion with ^{8}Be were significant, then the suppression of complete fusion would be even more than given in this paper. These fusion suppression factors are a simple, but unambiguous, way of demonstrating that fusion is reduced for nuclei which breakup easily in contrast with those which do not. If the measurements were to be compared with, for example, CDCC calculations where breakup and subsequent fragment motion were correctly modeled, there would be no suppression, as the predicted cross sections should match those measured.

The deduction of the suppression factors presented here depends on the variables that affect the calculated fusion cross sections at energies well above the average barrier. In this energy regime, in the case of nuclei which are well bound and do not breakup readily, the coupled channels predictions are close to the single barrier penetration calculations. This is because the barriers in the distribution, arising as a result of couplings, always cluster around the average barrier, i.e., the barriers are never widely separated. That this is expected is apparent from the fact that coupling strengths in nuclei are typically of the order of a few MeV and the average barrier energy is 10–100 times larger. Thus, in most situations the couplings are unlikely to introduce [36] large changes in the barrier energies or radii. The calculated cross sections much above the barrier are thus virtually independent of couplings, as long as the average barrier matches that determined experimentally.

Thus, at above-barrier energies, the calculated cross sections for nuclei which do not breakup depend primarily on the average barrier energy and radius. The latter, in turn, depends on the shape of the nuclear potential, and if the centroid of the experimental barrier distribution is reproduced, is determined largely by the diffuseness parameter of the commonly used Woods-Saxon potential. The uncertainties in the energy of the centroid of the barrier distribution (or equivalently the uncertainty in B_0) and the diffuseness parameter are therefore reflected in the uncertainties of the deduced suppression factors, as discussed later in this section.

The suppression of fusion can also be determined by comparing the measured and calculated area under the barrier distribution since it is approximately equal [37] to the geometrical cross-section πR_0^2 for the reaction. The suppression determined using this method is independent of the exact nature of the couplings, since the inclusion of couplings changes the shape of the barrier distribution but preserves the area under it. Using the cross sections for $E_{\mathrm{c.m.}} < 36$ MeV, the area for ^{6}Li is 64^{+4}_{-3}% and for ^{7}Li is 76 ± 2% of the model predictions. For ^{9}Be the measured area is 70 ± 5% of that calculated using the data for $E_{\mathrm{c.m.}} < 45$ MeV. The reductions obtained from the data around the average barrier energies are very close to those obtained from the high energy data. Yet another method of obtaining the suppression factor, which is fairly model independent, is presented in Sec. VIII E.

A. Energy dependence of the suppression factors

The ratio of measured complete fusion cross sections to those from the single barrier penetration calculations and the coupled channels model calculations are shown in Fig. 14 for the three systems using data at the high energies, where the measured barrier distribution has returned close to zero. The ratios for no couplings and including couplings are in agreement with each other, demonstrating that the effects of couplings to bound states are minimal at such high energies, and as expected the fusion suppression above the barrier is insensitive to the couplings (to bound states) as long as the centroids of the calculated barrier distributions matches that of the measured distribution. The above-barrier fusion suppression factors for all three systems remain constant with energy. Furthermore, as discussed above, these suppression factors match those determined using the area under the measured barrier distributions (shown by triangles in Fig. 14), that make use of cross-sections around the barrier energies. This implies that the fusion suppression remains remarkably constant with energy from B_0 to $1.7B_0$. This is a surprising result, as *a priori* one may expect the breakup probability, and hence its effect on fusion, to be energy dependent.

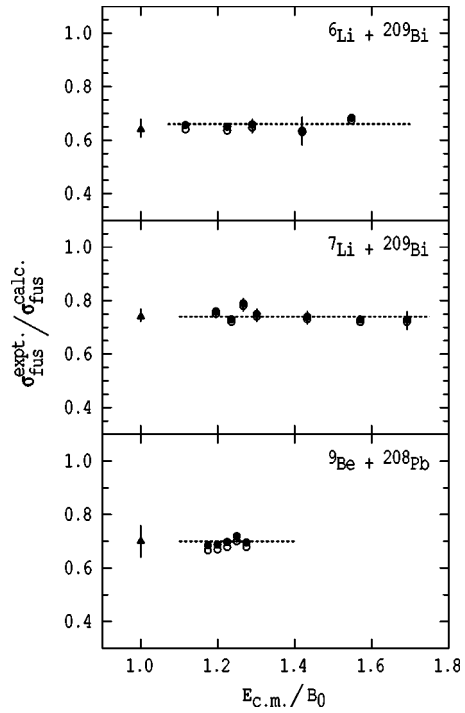

FIG. 14. Energy dependence of the suppression factors for above-barrier complete fusion for the three systems, as indicated. The open and filled circles represent the ratios obtained using the predictions of a single barrier penetration model and coupled channels calculations, respectively. The dashed line is the adopted suppression factor obtained by taking the average of the filled circles. The suppression factor obtained by comparison of the areas under the barrier distributions is shown by a triangle (plotted at $E_{\mathrm{c.m.}}/B_0 = 1.0$) in each panel.

B. Sensitivity of suppression factor to average barrier energy

The effect of changing the average barrier energy determined from the centroid of the barrier distribution (Sec. VI B), within its measured uncertainties was investigated.

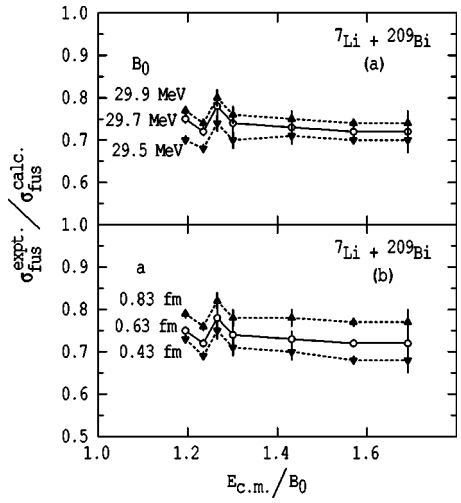

FIG. 15. The effect on the suppression factor for complete fusion due to change in (a) the fusion barrier energy and (b) the diffuseness parameter chosen for the Woods-Saxon nuclear potential for the ^{7}Li+^{209}Bi system.

For simplicity, single barrier penetration calculations, rather than the coupled channels calculations, were used for this purpose, as it has been shown (see Fig. 14) that the suppression factor hardly depends on the calculation used. The calculated average barrier energy was changed by one standard deviation of the experimental barrier uncertainty for each system by adjusting the depth of the Woods-Saxon potential. SBP calculations of the fusion cross-sections were carried out. The ratios of the measured complete fusion cross-sections to the predictions using different values of the barrier energies are shown for ^{7}Li+^{209}Bi in Fig. 15(a) as a function of center of mass energy divided by the experimentally determined B_0. The solid line joins the points obtained using the adopted average barrier energy, while the dashed lines join the points obtained using the maximum (up triangles) and minimum (down triangles) values. Calculations using the highest barrier energy give the least suppression, as expected. The uncertainties in the energy of the average barrier typically contribute ~90% to the total experimental uncertainty in the suppression factors for the three systems.

C. Sensitivity of suppression factor to the diffuseness parameter

The calculations presented thus far used a value of diffuseness parameter $a=0.63$ fm, as given by Woods-Saxon parametrization [32] of the Akyüz-Winther potential. However, theoretical fits to precise fusion excitation functions at above-barrier energies for heavy nuclei consistently require the diffuseness of 0.8 fm to ~1 fm, which appears to scale [38,39] with the charge product of the target and projectile. The present systems have a small charge product and the maximum value of diffuseness can be expected to be ~0.8 fm. The effect on the suppression factor of changing a by ±0.2 fm was therefore investigated using SBP calculations. Changing the diffuseness parameter essentially changes the slope of the high-energy cross sections and calculations using a larger diffuseness would be expected to show a slower increase of cross sections with energy. For a fixed value of a, the potential parameters were varied so that the measured B_0 was reproduced in each case. The ratio of the measured CF cross sections at high energies to those calculated for different values of a was determined for all three systems, and are shown in Fig. 15(b) for the ^{7}Li +^{209}Bi reaction. The full line joins the points obtained using $a=0.63$ fm in the calculations, while the dashed lines join the points obtained using a value of $a=0.43$ fm (down triangles) and 0.83 fm (up triangles). The uncertainties in the suppression factors given previously do not include the effect of changing the diffuseness parameter as this is not an experimental uncertainty. For the range of a of ±0.2 fm, the spread in average suppression factors is ±0.03, $^{+0.05}_{-0.03}$, and ±0.03, respectively, for the ^{6}Li, ^{7}Li, and ^{9}Be induced reactions.

D. Suppression factor for different projectiles

The suppression factors presented have been determined using two methods (Sec. VIII); the first uses the measured cross-sections at above-barrier energies and the second uses the area under the barrier distribution. The suppressions for the three reactions ^{6}Li+^{209}Bi, ^{7}Li+^{209}Bi, and ^{9}Be+^{208}Pb, respectively, using the first method are 66^{+5}_{-4}%, 74^{+3}_{-2}%, and 70^{+8}_{-7}%; while using the area yields 64^{+4}_{-3}%, 74^{+3}_{-2}%, and 70±6%. As discussed in the beginning of Sec. VIII, the relative suppression of ^{6}Li to ^{7}Li is much better determined and is measured to be 0.89±0.02. Although the suppression of the CF cross sections are similar for the different systems, the strongest CF suppression occurs for the ^{6}Li projectile, which has the lowest threshold against breakup (1.47 MeV), and the smallest suppression occurs for ^{7}Li, which has a higher breakup threshold of 2.47 MeV. The suppression for the ^{9}Be reaction, which has a threshold of 1.57 MeV and 2.47 MeV against breakup into 2α and a neutron, and ^{4}He and ^{5}He, respectively, is intermediate between the above two. This may lead to the simplistic picture that the suppression increases with a decreasing breakup threshold. However, the probability of breakup depends on the couplings to the continuum and to states above the breakup threshold, and also on the Coulomb barriers encountered by the breakup fragments. The coupling strengths in turn depend on the nuclear structure and the charge product of the target and projectile. The low charge product in reactions of Li with low-Z targets explains the observation of no fusion suppression in these reactions [46–49].

E. Suppression determined from cross-bombardment measurements

The fact that the high energy cross sections are suppressed can be seen, in a fairly model independent way, by comparing the cross sections for forming the same compound nucleus using projectiles which break up easily and those which do not. This makes use of the relationship $\sigma_{\rm fus} = \pi R^2(1-B_0/E_{\rm c.m.})$, which describes well the above-barrier cross sections. The different barrier radii and barrier energies for the different reactions can be normalized by dividing the

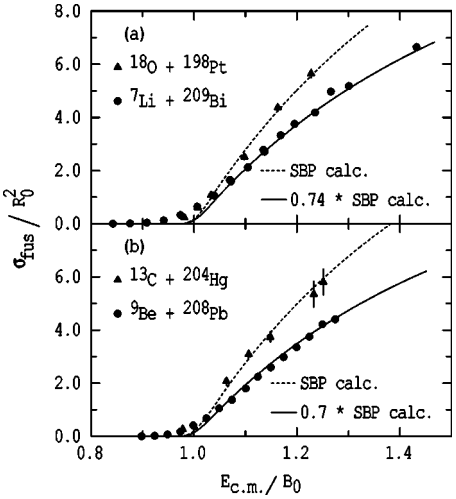

FIG. 16. Experimental reduced CF cross sections for (a) the ^{7}Li+^{209}Bi and ^{18}O+^{198}Pt reactions and (b) the ^{9}Be+^{208}Pb and ^{13}C+^{204}Hg reactions. These show that CF cross sections for reactions involving projectiles which break up readily are substantially lower than for reactions of well-bound nuclei. The dashed lines are the single barrier penetration model calculations which describe the data for the ^{18}O+^{198}Pt and ^{13}C+^{204}Hg reactions. The full lines are the result of multiplying the dashed lines by the factors indicated.

fusion cross sections by the square of the $l=0$ barrier radius R_0, and the $E_{\mathrm{c.m.}}$ by B_0. The fusion excitation functions (the sum of the Rn product nuclei and fission) divided by R_0^2 for the ^{9}Be+^{208}Pb and ^{13}C+^{204}Hg systems, leading to the compound nucleus ^{215}Rn, and for the ^{7}Li+^{209}Bi and ^{18}O+^{198}Pt systems, both leading to the compound nucleus ^{216}Rn, are compared in Fig. 16. The barrier radii and B_0 for the ^{18}O and ^{13}C induced reactions are obtained from the SBP calculations (dashed lines), which describe the data well. For the lighter projectiles, the barrier radius and energy are those of the SBP calculations discussed in Sec. VII A. The full lines in Fig. 16 are obtained by multiplying the dashed lines by the suppression factors of 0.74 and 0.70 for the ^{7}Li and ^{9}Be systems obtained in Sec. VIII. They are in close agreement with the high energy data for the ^{7}Li and ^{9}Be induced reactions. This demonstrates that above-barrier fusion cross sections for reactions involving nuclei which break up easily are suppressed by the same amount, independent of whether the comparison is made with theoretical expectations or with experimental measurements involving nuclei which do not break up readily.

IX. INCOMPLETE FUSION

The complete fusion data clearly indicate that the fusion above the average barrier is significantly reduced for all three systems, each involving a projectile which readily breaks up. In a classical picture this reduction would imply that a significant number of projectile trajectories, which would normally have led to complete fusion, resulted in some other process. Breakup of the projectiles appears as an obvious explanation, and should manifest itself by large prompt breakup cross sections, as indeed was seen in a recent investigation [26] of the reaction of ^{9}Be with Pb.

TABLE V. *Q*-values for three most energetically favorable breakup partitions for ^{6}Li, ^{7}Li, and ^{9}Be, and the products following capture of the each of the fragments by the target.

Projectile	Breakup fragments	*Q*-value (MeV)	Capture products
^{6}Li	^{4}He+^{2}H	−1.475	^{213}At,^{211}Po
	^{5}He+^{1}H	−4.594	^{214}At,^{210}Po
	^{5}Li+n	−5.666	^{214}Rn[a],^{210}Bi[b]
^{7}Li	^{4}He+^{3}H	−2.467	^{213}At,^{212}Po
	^{6}Li+n	−7.249	^{215}Rn[a],^{210}Bi[b]
	^{5}He+^{2}H	−9.618	^{214}At,^{211}Po
^{9}Be	^{4}He+^{4}He+n	−1.573	^{212}Po,^{209}Pb[b]
	^{8}Be+n	−1.665	^{216}Rn[a],^{209}Pb[b]
	^{5}He+^{4}He	−2.467	^{213}Po,^{212}Po

[a]Cannot be separated from complete fusion.
[b]Alpha decay branch very small or does not decay by α-emission.

The three most energetically favorable breakup partitions for the ^{6}Li, ^{7}Li, and ^{9}Be nuclei are given in Table V. The other breakup channels in all cases require energies $\geqslant$10 MeV. For all three nuclei, break up into charged fragments is energetically most favorable. Indeed, experiments with ^{6}Li and ^{7}Li incident on ^{208}Pb targets clearly show their breakup into the energetically favored partitions of α-^{2}H [40] and α-^{3}H [41] nuclei, respectively. At energies near and above the barrier, the breakup fragments can be captured by the target, resulting in incomplete fusion. Products resulting from this process are given later in column (iv) of Table XI for the present systems. Amongst them, those which are formed by the capture of a charged fragment of the projectile can be distinguished from complete fusion since they have different Z, and the CN formed following CF does not significantly decay by charged particle emission. Furthermore, in the present cases an unambiguous identification is relatively simple as the ICF products are α-active. If, instead, the breakup results in a neutron and only one other charged fragment (as is predominantly the case for ^{6}He,^{8}He,^{11}Be nuclei) and the latter is captured by the target, then it cannot be distinguished from complete fusion, as all of the charge of the projectile is captured. Such events are included in the complete fusion cross sections. The capture of the neutron alone by the target leads to a stable nucleus in our measurements, and therefore these ICF events cannot be detected by the decay α technique used here.

The cross sections for α-active incomplete fusion products of Po,At are listed in Tables VI–VIII, for the ^{6}Li +^{209}Bi, ^{7}Li+^{209}Bi, and ^{9}Be+^{208}Pb systems, respectively, and the corresponding excitation functions are shown in Figs. 17–19. The cross sections for ^{211}Bi, a transfer product (see Sec. IV B) in the reaction of ^{7}Li with ^{209}Bi, are also given in Table VII, and shown in Fig. 18 by the hollow circles. The cross sections for ^{212}At and ^{211}Po nuclei given in the tables and figures are the sum of their ground state and isomeric state cross sections. The cross sections for ^{210}Po in Fig. 19 have large error bars at the lower energies because of the subtraction of the large contribution from the decay of the CF product ^{214}Rn.

TABLE VI. Measured cross sections for incomplete fusion products resulting from the reaction of ^{6}Li with ^{209}Bi. The last column is the sum of the individual cross sections. The cross sections for ^{209}Po, which may be significant at the high energies, could not be measured due to its long half-life.

$E_{c.m.}$ (MeV)	^{213}At (mb)	^{212}At (mb)	^{211}At (mb)	^{212}Po (mb)	^{211}Po (mb)	^{210}Po (mb)	ΣAt+ΣPo (mb)
25.13							
26.16							
27.11	0.22±0.09	1.40±0.16					
28.06	0.94±0.13	3.56±0.24	0.51±0.10				
29.08	1.14±0.20	8.10±0.39	1.85±0.22			61.2±7.5	72.3±7.5
30.04	2.15±0.23	14.3±0.5	3.50±0.24			63±10[a]	83±10
30.98	3.46±0.26	21.8±0.7	6.80±0.30	0.21±0.08		65±10[a]	97±10
32.00	4.38±0.37	29.1±1.0	13.8±0.7	0.39±0.13		66.5±10[a]	114±10
32.96	4.89±0.36	36.2±0.9	19.9±0.7	0.50±0.15[a]		68.6±8.7	130.1±8.8
34.92	5.94±0.36	46.2±1.0	41.4±1.2	0.63±0.12		70.5±10[a]	165±10
36.86	5.73±0.37	51.8±1.1	66.8±2.2	0.74±0.14		72.6±8.7	197.7±9.0
38.81	4.58±0.37	54.2±1.1	89.6±3.9	0.75±0.16[a]	1.8±0.3	84±10[a]	235±11
42.70	4.15±0.37	45.4±1.1	144±22	0.75±0.16	3.49±0.46	105±23	303±32
46.58	2.42±0.29	33.5±0.5	173.3±8.8	1.30±0.22	4.71±0.17	336±22	551±24

[a]Interpolated value.

For the ^{6,7}Li induced reactions, ICF results in many different isotopes of Po and At. The cross sections for a few of them could either not be determined or could not be determined individually, as discussed below. The nucleus ^{210}At, resulting from *n*-evaporation from the combined system formed by ICF, decays almost completely (99.82%) by EC $+\beta^{+}$ to ^{210}Po, with $T_{1/2}=8.3$ h. The cross section of ^{210}Po ($T_{1/2}=138$ days) was obtained from off-line spectra accumulated a few days after the irradiations (see Sec. II A) and nearly all of the ^{210}At would be expected to have decayed to

TABLE VII. Measured cross sections for incomplete fusion products resulting from the reaction of ^{7}Li with ^{209}Bi. The cross sections for ^{211}Bi resulting from two neutron stripping is also given. The last column is the sum of the individual At and Po cross sections. The cross sections for ^{209}Po, which may be significant at the high energies, could not be measured due to its long half-life.

$E_{c.m.}$ (MeV)	^{213}At (mb)	^{212}At (mb)	^{211}At (mb)	^{212}Po (mb)	^{211}Po (mb)	^{210}Po (mb)	^{211}Bi (mb)	ΣAt+ΣPo (mb)
25.02					1.58±0.18			
26.01					3.84±0.25			
26.98					9.07±0.37			
27.95	0.77±0.53	1.06±0.13			15.2±0.5		0.43±0.09	
28.92	1.62±0.50	3.24±0.23			22.9±0.7	74±5	0.68±0.12	102±5
29.89	4.00±1.03	7.12±0.40			28.7±0.8	100±15[a]	1.17±0.17	140±15
30.86	4.90±1.01	11.4±0.5		0.54±0.15	35.0±0.9	130±15[a]	1.89±0.24	182±15
31.83	6.81±1.41	17.1±0.7		0.80±0.20	36.4±1.1	160±15[a]	2.66±0.33	221±15
32.80	6.41±0.83	21.6±0.8		1.48±0.27	39.2±1.2	192±12	4.04±0.41	261±12
33.77	8.33±0.46	24.2±0.8		1.82±0.30	37.9±1.2	200±30[a]	5.1±0.5	272±30
34.70	10.2±0.9	24.4±1.3	4.50±0.60	2.59±0.57	37.1±1.6	200±30[a]	5.7±0.7	279±30
36.68	13.3±0.9	25.4±1.4	15±4[a]	2.66±0.54	33.9±1.7	200±30[b]	7.3±0.6	290±30
38.63	15.5±1.5	27.6±1.1	21.7±2.0	2.32±0.41	31.7±1.3	203±21	9.0±0.8	302±21
42.53	19.7±1.8	31.5±1.5	44.1±3.1	1.87±0.44	23.9±1.4	194±25	9.3±1.0	315±25
46.38	19.4±0.9	43.9±1.5	51.0±4.0	1.55±0.30	22.2±1.1	191±83	9.3±0.8	329±83
50.23	14.4±0.6	47.5±1.3	83.0±5.0	1.27±0.27	19.6±0.9	200±30[a]	8.8±0.7	366±30

[a]Interpolated value.
[b]Extrapolated value.

TABLE VIII. Measured cross sections for incomplete fusion products resulting from the reaction of ^{9}Be with ^{208}Pb. The last column is the sum of the individual cross sections.

$E_{c.m.}$ (MeV)	^{212}Po (mb)	^{211}Po (mb)	^{210}Po (mb)	ΣPo (mb)
34.40	0.77±0.20	0.65±0.31		1.42±0.37
35.37	1.81±0.33	1.03±0.59		2.84±0.68
36.33	4.62±0.76	8.2±1.2		12.8±1.4
37.29	8.92±0.97	20.8±1.9		29.7±2.1
38.25	10.9±0.9	35.6±2.4		46.5±2.6
39.22	14.3±1.0	57.4±2.5	3.3±11	75±11
40.16	13.4±1.1	72.7±3.2	8±10[a]	94±11
41.12	13.5±1.3	92.9±4.0	13±20	119±20
42.15	13.6±1.2	114.3±3.7	22±20[a]	150±20
43.05	14.7±1.3	131.2±4.5	32±25	178±25
44.01	15.6±1.6	142.8±4.9	32±20[a]	190±21
44.96	15.5±1.6	144.0±4.9	32±20[a]	192±21
45.92	15.7±1.9	147.2±5.2	32±14	195±15
46.88	13.6±1.6	150.0±5.2	52±20[a]	216±21
47.84	11.7±1.6	146.3±4.9	73±20[a]	231±21
48.80	12.3±1.7	145.1±5.3	94±17	251±18

[a]Interpolated value.

^{210}Po by then. Thus the individual cross sections for ^{210}Po and ^{210}At could not be obtained, and the summed yield is given.

The sizable population of ^{211}Po and ^{210}Po leads to the expectation of a substantial population of ^{209}Po. The cross sections for this nucleus could not be determined in the present experiments due to its long half-life of 102 years. The code PACE [42] was used to get a qualitative idea of the importance of this channel. In order to estimate the energy of the deuteron (triton), to use as input in the code, a very simple energy sharing assumption was made; the available energy $E_{c.m.}+Q_{breakup}$ was divided equally among the six

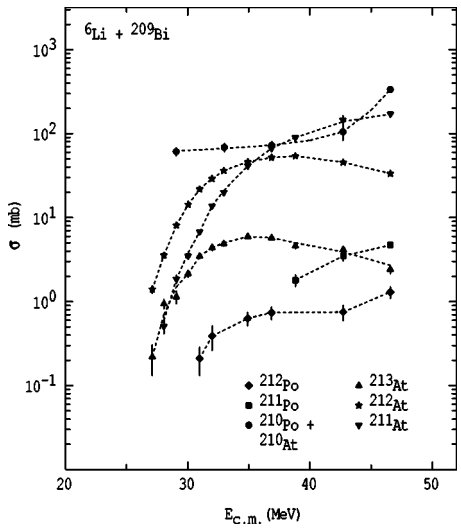

FIG. 17. The measured ICF cross sections for the ^{6}Li+^{209}Bi system. The lines are to guide the eye.

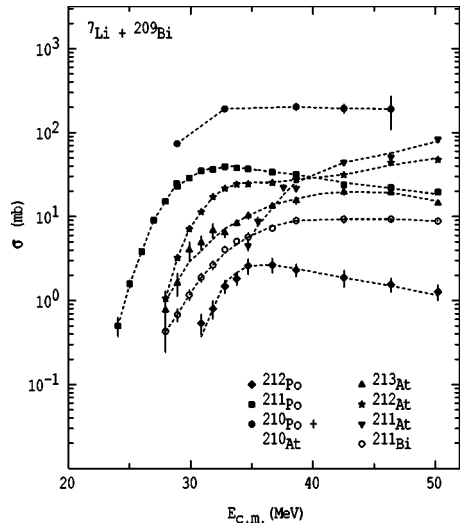

FIG. 18. The measured ICF cross sections for the ^{7}Li+^{209}Bi system. Also shown are the cross sections for ^{211}Bi, likely to have resulted from the transfer of neutrons to the target. The lines are to guide the eye.

(seven) nucleons, and their relative kinetic energy was neglected. So, the deuteron (triton) gets half (3/4) of the α-particle energy. With such a simple picture, the code predicts that for ^{6}Li the ^{209}Po channel becomes important at medium and high energies, having cross sections larger than that of ^{210}Po at the highest energies. For ^{7}Li the predictions are similar, the ^{209}Po channel is important for the three or four highest energies, with cross sections larger than the ^{210}Po channel for the two highest energies. The last column of Tables VI and VII give the summed cross sections for the observed Po and At nuclei. This cross section is only a lower limit to the total ICF cross section, particularly for energies above 36 MeV, since the sum does not include the cross sections for ^{209}Po.

Compared with ^{6,7}Li, the ICF of ^{9}Be produces fewer nuclei as the two charged fragments have the same Z. Figure 19

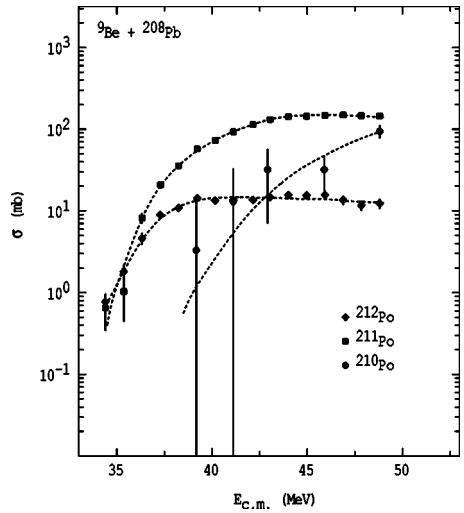

FIG. 19. The measured ICF cross sections for the ^{9}Be+^{208}Pb system. The lines are to guide the eye.

shows that the cross section for ^{210}Po is continuously increasing up to the highest measured energy; only here does it make a significant contribution to σ_{ICF}. Thus a substantial population of ^{209}Po is not expected. This conclusion is supported by the calculations from the statistical model code PACE (described above) which agree qualitatively with the data and do not predict the presence of ^{209}Po. Thus, for the energy range of the current measurements, the sum of ^{212}Po, ^{211}Po, and ^{210}Po would be expected to exhaust the total incomplete fusion cross section following absorption of ^{4}He (or ^{5}He). The summed cross sections of these channels are given in the last column of Table VIII.

The summed incomplete fusion cross sections are typically 50% of the measured complete fusion cross sections, and are very similar to the cross section missing from complete fusion. This appears to fulfill the simple expectations that the flux loss from complete fusion at above-barrier energies appears as incomplete fusion. However, this deduction may be clouded by the fact that experimentally it is difficult to separate transfer contributions from incomplete fusion, as will be discussed in Sec. X A.

X. CONTROVERSIES IN FUSION WITH WEAKLY BOUND LIGHT PROJECTILES

The effect of the weak binding of nuclei on fusion has been the subject of many controversies in the past. Some of these controversies are related to theoretical descriptions of the effect of breakup, some others are mainly due to experimental difficulties in identification of complete fusion and separating it from incomplete fusion. These issues are discussed below.

A. Enhancement or suppression of complete fusion with heavy target nuclei

Until recently, there were two opposing theoretical points of view, one which predicted the enhancement of fusion cross sections due to couplings to the low lying unbound or continuum states of the weakly bound light nuclei [12,13], and the other which predicted reduction in fusion due to break up of the nuclei [11,10]. However, it was shown recently [14], that complete fusion cross sections are enhanced at energies below the barrier but reduced at above-barrier energies. Since then this result has been supported by other theoretical calculations [15]. Thus, the question of enhancement versus suppression is resolved as far as theoretical predictions are concerned. However, most of the calculations are qualitative, and a quantitative understanding of the processes of complete and incomplete fusion continues to be a challenge.

Experimentally the question of enhancement and suppression appears to be controversial due to the fact that different studies have concentrated on different energy regimes. The discussion above makes it clear that it is important to always make clear whether the measurements are below or above the fusion barrier. Thus the claims of large sub-barrier enhancement of fusion cross sections for ^{6}He+^{209}Bi [2] and ^{6}He+^{238}U [7] may not be in conflict with the above-barrier suppression of complete fusion that is observed in the present reactions. For ^{6,7}Li+^{209}Bi and ^{9}Be+^{208}Pb, the complete fusion is enhanced compared to single barrier expectations at energies below the barrier, though the enhancement is not as significant as in the ^{6}He induced reactions, where couplings to *n*-transfer [2] may play a significant role in enhancing fusion at low energies. Such a large influence of *n*-transfer is most likely due to the extended wavefunctions of the loosely bound neutrons in ^{6}He.

Which products should be included in the experimentally determined complete fusion cross sections is another potential problem. For example it is not possible to separate the fusion of ^{9}Be from that of ^{8}Be since the energy of the neutron, following breakup close to the barrier, is similar to the energy carried by an evaporated neutron. Therefore, ^{216}Rn formed following the evaporation of one neutron from the CN formed by fusion of ^{9}Be has an excitation energy very similar to that of ^{216}Rn which is formed by the incomplete fusion of ^{8}Be. The resulting ERs are therefore very similar and hence cannot be identified separately as CF and ICF. A similar problem occurs for the fusion of ^{11}Be, which is difficult to distinguish [1] from that of ^{10}Be.

If the probability of breakup into one charged fragment and neutrons is very large, then the cross section for the capture of the fragment with charge equal to Z_P may be expected to be large. The inclusion of such events could well lead to apparently large complete fusion yields, which might mean that the above-barrier suppression of "true" complete fusion would not be observed experimentally. Thus, in the fusion reactions with nuclei such as ^{6,8}He, ^{11}Li, and ^{11}Be, which predominantly break up into a charged fragment and neutrons, it is important to know and specify whether the experimental complete fusion cross sections include or exclude contributions from the capture of ^{4}He, ^{10}Li, and ^{10}Be (or ^{9}Be). This knowledge is essential and has to be kept in mind while arriving at conclusions about the enhancement or suppression relative to the calculations or results obtained from their stable counterparts.

B. The "total" fusion cross sections

The sum of experimentally determined complete and incomplete fusion cross sections, referred to as the "total" fusion cross section, has sometimes been compared with theoretical calculations. Breakup does not significantly affect the total cross sections at energies above the barrier, since CDCC calculations including the effects of breakup closely match [43] those without breakup. For the Li induced reactions, the "total" fusion cross sections at above-barrier energies agree with CDCC predictions [43] which include the effect of breakup. This is not unexpected since it was already mentioned in Sec. IX that the total incomplete fusion cross sections are similar to the observed deficit of CF. However, the summing of CF and ICF cross sections may not be a valid measure of "total" fusion, as the latter may include contributions from transfer.

At energies below the barrier, a distinction between breakup and transfer may be made experimentally by observing the outgoing fragments, since the detection of all frag-

ments can be identified as breakup, whereas in the case of transfer only a part of the projectile would be observed. At energies above the barrier, the breakup fragments may have sufficient energy to overcome the Coulomb barrier and get captured by the target, resulting in the same product as transfer. For example, the Po and At nuclei formed in the case of a ^{6}Li induced reaction by breakup-capture can also be formed by the transfer of p, d, or α to the target. Thus, even if it is assumed that in theory (for example, based on impact parameter considerations), a distinction between the processes of transfer and breakup followed by capture is possible, it is difficult to do so experimentally for light projectiles such as ^{6,8}He, Li, or Be.

The present experiment therefore cannot distinguish between transfer and incomplete fusion. While this does not affect the conclusions of the paper, nevertheless it is useful to have an estimate of the contribution of transfer in incomplete fusion before a comparison with theoretical calculations are made. The only clear case of transfer observed in the present experiment is the production of ^{211}Bi ($2n$ transfer, $Q=-3.171$ MeV), with a cross section of $\sim$10 mb, for the ^{7}Li induced reaction (see Sec. IV B). However, this cannot be taken as a typical order of magnitude for transfer as first it is the transfer of two nucleons, which is known to have a probability smaller than one nucleon transfer, and second it cannot be used to estimate the cross sections for the transfer of clusters such as α and t. It would therefore be very useful to have a theoretical estimate of the cross sections for the transfer of clusters, particularly those which are used in the cluster model description of the projectile.

In the case of reactions with very heavy targets such as ^{238}U, where the CN decays by fission, the separation even of complete fusion from transfer can pose difficulties. A recent measurement of the reaction of ^{6}He with ^{238}U found large cross sections for neutron transfer induced fission [44], which were previously not distinguished from complete fusion—fission [7], leading to apparently large complete fusion cross sections.

C. Fusion of weakly bound light nuclei with low-Z targets

Reactions of weakly bound light nuclei with targets ranging from $Z=3$ to $Z\sim30$ have recently been the subject of many investigations [45–48,50,51]. In most of the cases the (total) fusion cross sections do not show significant effects of breakup on fusion, i.e., neither substantial enhancement below the barrier nor reduction above the barrier was found. This apparent "absence" of suppression or enhancement is not in contradiction with the results of fusion with heavy targets. Fusion with light nuclei results in CN which also evaporate charged particles in addition to neutrons. Thus even when the projectiles break up into charged partitions (a favorable case for the identification of ICF for heavy CN), the ICF products are identical to the evaporation residues following charged particle emission from the CN. Thus it is almost impossible, in a model independent way, to separate the products of complete fusion from incomplete fusion. This is particularly so at energies above the barrier whereas at below-barrier energies the lack of sufficient energy may prohibit incomplete fusion. Therefore, in all of the investigations with low-Z targets, the sum of complete and incomplete fusion (or the "total" fusion) is obtained, and compared with theoretical expectations. However, as discussed in Sec. X B, the "total" fusion cross section is not expected to be significantly suppressed at above-barrier energies, which is entirely consistent with the experimental observations.

The question may be asked as to whether the results would be any different if complete and incomplete fusion could be separated. A recent study [26] predicted that complete fusion suppression at energies above the barrier is almost proportional to the charge of the target nuclei. A suppression of $\sim$4% for ^{9}Be+^{19}F [48] and 13% for ^{9}Be+^{64}Zn [46] was predicted [26], which is well within the experimental uncertainties of the existing measurements. Thus, even if complete fusion could be separated, the suppression might be expected to be much smaller than for the high-Z targets.

XI. SUMMARY AND OUTLOOK

The complete and incomplete fusion excitation functions for the reactions of ^{6}Li and ^{7}Li with ^{209}Bi and of ^{9}Be with ^{208}Pb have been measured from below-barrier to above-barrier energies. At energies below the fusion barrier, there is a small enhancement in the cross sections, compared with the predictions of a single barrier model, consistent with the low charge product of the reacting nuclei. However, at energies above the barrier the complete fusion cross sections are suppressed by $\sim$30% compared with the expectations for fusion without breakup. An almost model independent demonstration of this suppression was presented by comparing the complete fusion cross sections for the pairs of reactions ^{7}Li+^{209}Bi and ^{18}O+^{198}Pt forming ^{216}Rn and ^{9}Be+^{208}Pb and ^{13}C+^{204}Hg, forming ^{217}Rn. The observed suppression of complete fusion is associated with projectiles with low energy threshold against breakup which allows them to break up prior to reaching the fusion barrier. This is supported by the large incomplete fusion cross sections observed for all three reactions.

It is pointed out that a separation of complete fusion from incomplete fusion (and transfer) is important for meaningful conclusions about the effect of breakup of nuclei on fusion. Misunderstandings or controversies about the enhancement/suppression of fusion from an experimental point of view have resulted in part from the differences in what is included in the measured complete fusion cross sections, and also from the fact that various works have concentrated on different energy regimes with respect to the barrier. The above-barrier suppression of complete fusion seen here is not in contradiction with the below-barrier enhancement seen in fusion with radioactive beams (due in the latter reactions largely to couplings to transfer channels). In the latter category of reactions, either the measurements have not extended far above the barrier for suppression to be observed, or the complete fusion measurements have included incomplete fusion and/or transfer, thus giving an apparently large fusion yield. The fusion suppression at above-barrier energies is only with respect to calculations which do not include breakup, and not with respect to realistic quantum mechani-

cal calculations which include the effect of couplings to bound, unbound, and continuum states. Such calculations should be able to predict the observed complete fusion cross sections.

A lot of progress has recently been made in theoretical modeling of fusion of light nuclei having low breakup threshold energies, and the past theoretical controversies have, at least qualitatively, been resolved. It is now clear that the complete fusion cross sections at energies below the barrier will be enhanced due to couplings to bound and unbound (and transfer) states, but suppressed at energies above the barrier due to break up of the weakly bound light nucleus. However, thus far the models have either been qualitative, or have not attempted to separate complete fusion from incomplete fusion cross sections. A separation of these processes requires the calculations to follow the projectile fragments up to their end point. This is not currently incorporated in any model, and remains a challenge for future realistic models of fusion of nuclei which readily break up.

ACKNOWLEDGMENTS

The work of M.D. was supported by the Australian Research Council. The Brazilian authors received partial support from CNPq, CAPES, FAPESP, and FAPERJ.

[1] A. Yoshida, C. Signorini, T. Fukuda, Y. Watanabe, N. Aoi, M. Hirai, M. Ishihara, H. Kobinata, Y. Mizoi, L. Mueller, Y. Nagashima, J. Nakano, T. Nomura, Y. H. Pu, and F. Scarlassara, Phys. Lett. B **389**, 457 (1996).

[2] J. J. Kolata, V. Guimarães, D. Peterson, P. Santi, R. White-Stevens, P. A. DeYoung, G. F. Peaslee, B. Hughey, B. Atalla, M. Kern, P. L. Jolivette, J. A. Zimmerman, M. Y. Lee, F. D. Becchetti, E. F. Aguilera, E. Martinez-Quiroz, and J. D. Hinnefeld, Phys. Rev. Lett. **81**, 4580 (1998).

[3] C. Signorini, Z. H. Liu, A. Yoshida, T. Fukuda, Z. C. Li, K. E. G. Löbner, L. Müller, Y. H. Pu, K. Rudolph, F. Soramel, C. Zotti, and J. L. Sida, Eur. Phys. J. A **2**, 227 (1998).

[4] K. E. Rehm, H. Esbensen, C. L. Jiang, B. B. Back, F. Borasi, B. Harss, R. V. F. Janssens, V. Nanal, J. Nolen, R. C. Pardo, M. Paul, P. Reiter, R. E. Segel, A. Sonzogni, J. Uusitalo, and A. H. Wuosmaa, Phys. Rev. Lett. **81**, 3341 (1998).

[5] K. E. Zyromski, W. Loveland, G. A. Souliotis, D. J. Morrissey, C. F. Powell, O. Batenkov, K. Aleklett, R. Yanez, I. Forsberg, M. Sanchez-Vega, J. R. Dunn, and B. G. Glagola, Phys. Rev. C **55**, R562 (1997).

[6] M. Dasgupta, D. J. Hinde, R. D. Butt, R. M. Anjos, A. C. Berriman, N. Carlin, P. R. S. Gomes, C. R. Morton, J. O. Newton, A. S. Toledo, and K. Hagino, Phys. Rev. Lett. **82**, 1395 (1999).

[7] M. Trotta, J. L. Sida, N. Alamanos, A. Andreyev, F. Auger, D. L. Balabanski, C. Borcea, N. Coulier, A. Drouart, D. J. C. Durand, G. Georgiev, A. Gillibert, J. D. Hinnefeld, M. Huyse, C. Jouanne, V. Lapoux, A. Lépine, A. Lumbroso, F. Marie, A. Musumarra, G. Neyens, S. Ottini, R. Raabe, S. Ternier, P. Van Duppen, K. Vyvey, C. Volant, and R. Wolski, Phys. Rev. Lett. **84**, 2342 (2000).

[8] V. Tripathi, A. Navin, K. Mahata, K. Ramachandran, A. Chatterjee, and S. Kailas, Phys. Rev. Lett. **88**, 172701 (2002).

[9] M. Dasgupta, D. J. Hinde, K. Hagino, S. B. Moraes, P. R. S. Gomes, R. M. Anjos, R. D. Butt, A. C. Berriman, N. Carlin, C. R. Morton, J. O. Newton, and A. S. Toledo, Phys. Rev. C **66**, 041602(R) (2002).

[10] M. S. Hussein, M. P. Pato, L. F. Canto, and R. Donangelo, Phys. Rev. C **46**, 377 (1992); Nucl. Phys. **A588**, 85c (1995); M. S. Hussein and A. F. R. de Toledo Piza, Phys. Rev. Lett. **72**, 2693 (1994).

[11] N. Takigawa, M. Kuratani, and H. Sagawa, Phys. Rev. C **47**, R2470 (1993).

[12] C. H. Dasso and A. Vitturi, Phys. Rev. C **50**, R12 (1994).

[13] K. Yabana, Prog. Theor. Phys. **97**, 437 (1997).

[14] K. Hagino, A. Vitturi, C. H. Dasso, and S. M. Lenzi, Phys. Rev. C **61**, 037602 (2000).

[15] A. Diaz-Torres and I. J. Thompson, Phys. Rev. C **65**, 024606 (2002).

[16] D. R. Zolnowski, H. Yamada, S. E. Cala, A. C. Kahler, and T. T. Sugihara, Phys. Rev. Lett. **41**, 92 (1978).

[17] K. Siwek-Wilczyńska, E. H. du Marchie van Voorthuysen, J. van Popta, R. H. Siemssen, and J. Wilczyński, Phys. Rev. Lett. **42**, 1599 (1979).

[18] A. C. Berriman, D. J. Hinde, M. Dasgupta, C. R. Morton, R. D. Butt, and J. O. Newton, Nature (London) **413**, 144 (2001).

[19] D. J. Hinde, M. Dasgupta, J. R. Leigh, J. C. Mein, C. R. Morton, J. O. Newton, and H. Timmers, Phys. Rev. C **53**, 1290 (1996).

[20] D. J. Hinde, A. C. Berriman, M. Dasgupta, J. R. Leigh, J. C. Mein, C. R. Morton, and J. O. Newton, Phys. Rev. C **60**, 054602 (1999).

[21] C. R. Morton, D. J. Hinde, J. R. Leigh, J. P. Lestone, M. Dasgupta, J. C. Mein, J. O. Newton, and J. O. Timmers, Phys. Rev. C **52**, 243 (1995).

[22] W. Stoeffl (unpublished); and T. Kibédi, ANU Internal Report, ANU-P/1226, 1997.

[23] G. D. Dracoulis, A. P. Byrne, T. Kibédi, T. R. McGoram, and S. M. Mullins, J. Phys. G **23**, 1191 (1997).

[24] T. R. McGoram, G. D. Dracoulis, A. P. Byrne, A. R. Poletti, and S. Bayer, Nucl. Phys. **A637**, 469 (1998).

[25] A. C. Berriman, Ph.D thesis, Australian National University, 2002.

[26] D. J. Hinde, M. Dasgupta, B. R. Fulton, C. R. Morton, R. J. Wooliscroft, A. C. Berriman, and K. Hagino, Phys. Rev. Lett. **89**, 272701 (2002).

[27] H. Freiesleben, H. C. Britt, J. Birkelund, and J. R. Huizenga, Phys. Rev. C **10**, 245 (1974).

[28] D. J. Hinde, M. Dasgupta, and A. Mukherjee, Phys. Rev. Lett. **89**, 282701 (2002).

[29] J. R. Leigh, M. Dasgupta, D. J. Hinde, J. C. Mein, C. R. Morton, R. C. Lemmon, J. P. Lestone, J. O. Newton, H. Timmers, J. X. Wei, and N. Rowley, Phys. Rev. C **52**, 3151 (1995).

[30] K. Hagino, N. Rowley, and A. T. Kruppa, Comput. Phys. Commun. **123**, 143 (1999).
[31] M. Dasgupta, D. J. Hinde, J. O. Newton, and K. Hagino, Prog. Theor. Phys. Suppl. (to be published).
[32] R. A. Broglia and A. Winther, *Heavy Ion Reactions Lecture Notes, Volume I: Elastic and Inelastic Reactions* (Benjamin/Cummings, Reading, 1981), p. 114.
[33] Ó. Akyüz and A. Winther, *Proceedings of the Enrico Fermi International School of Physics 1979*, edited by R. A. Broglia, C. H. Dasso, and R. Richi (North-Holland, Amsterdam, 1981).
[34] M. J. Martin, Nucl. Data Sheets **63**, 723 (1991).
[35] A. Navin (private communication, 2003).
[36] C. H. Dasso, *Proceedings of the XXII International Winter Meeting on Nuclear Physics*, Bormio, 1984, Nordita preprint, nordita-84/11.
[37] M. Dasgupta, D. J. Hinde, N. Rowley, and A. M. Stefanini, Annu. Rev. Nucl. Part. Sci. **48**, 401 (1998).
[38] J. O. Newton, C. R. Morton, M. Dasgupta, J. R. Leigh, J. C. Mein, D. J. Hinde, H. Timmers, and K. Hagino, Phys. Rev. C **64**, 064608 (2001).
[39] J. O. Newton *et al.*, Phys. Rev. C (to be published).
[40] D. Scholz, H. Gemmeke, L. Lassen, R. Ost, and K. Bethge, Nucl. Phys. **A288**, 351 (1977), and references therein.
[41] A. C. Shotter, A. N. Bice, J. M. Wouters, W. D. Rae, and J. Cerny, Phys. Rev. Lett. **46**, 12 (1981), and references therein.
[42] A. Gavron, Phys. Rev. C **21**, 230 (1980).
[43] A. Diaz-Torres, I. J. Thompson, and C. Beck, Phys. Rev. C **68**, 044607 (2003).
[44] M. Trotta (private communication).
[45] J. Takahashi, M. Munhoz, E. M. Szanto, N. Carlin, N. Added, A. A. P. Suaide, M. M. de Moura, R. Liguori Neto, A. Szanto de Toledo, and L. F. Canto, Phys. Rev. Lett. **78**, 30 (1997).
[46] S. B. Moraes, P. R. S. Gomes, J. Lubian, J. J. S. Alves, R. M. Anjos, M. M. Sant'Anna, I. Padron, C. Muri, R. Liguori Neto, and N. Added, Phys. Rev. C **61**, 064608 (2000).
[47] A. Mukherjee, M. Dasgupta, D. J. Hinde, H. Timmers, R. D. Butt, and P. R. S. Gomes, Phys. Lett. B **526**, 295 (2002).
[48] R. M. Anjos, C. Muri, J. Lubian, P. R. S. Gomes, I. Padron, J. J. S. Alves, G. V. Martí, J. O. Fernández Niello, A. J. Pacheco, O. A. Capurro, D. Abriola, J. E. Testoni, M. Ramírez, R. Liguori Neto, and N. Added, Phys. Lett. B **534**, 45 (2002).
[49] I. Padron, P. R. S. Gomes, R. M. Anjos, J. Lubian, C. Muri, J. J. S. Alves, G. V. Martí, M. Ramírez, A. J. Pacheco, O. A. Capurro, J. O. Fernández Niello, J. E. Testoni, D. Abriola, and M. R. Spinella, Phys. Rev. C **66**, 044608 (2002).
[50] A. Mukherjee and B. Dasmahapatra, Phys. Rev. C **63**, 017604 (2001).
[51] C. Beck, F. A. Souza, N. Rowley, S. J. Sanders, N. Aissaoui, E. E. Alonso, P. Bednarczyk, N. Carlin, S. Courtin, A. Diaz-Torres, A. Dummer, F. Haas, A. Hachem, K. Hagino, F. Hoellinger, R. V. F. Janssens, N. Kintz, R. Liguori Neto, E. Martin, M. M. Moura, M. G. Munhoz, P. Papka, M. Rousseau, A. Sànchez i Zafra, O. Stézowski, A. A. Suaide, E. M. Szanto, A. Szanto de Toledo, S. Szilner, and J. Takahashi, Phys. Rev. C **67**, 054602 (2003).